Prospects for Top Quark Mass Measurement Through the Fully Hadronic Decay of Top-Antitop Events with the ATLAS Detector

by

Keith Edmonds
B.Sc. (Honours) University of British Columbia 2005

A Thesis Submitted in Partial Fullfillment of the
Requirements for the Degree of

MASTER OF SCIENCE

in the Department of Physics and Astronomy

Prospects for Top Quark Mass Measurement Through the Fully Hadronic Decay of Top-Antitop Events with the ATLAS Detector

By

Keith Edmonds

B.Sc. (Honours) University of British Columbia 2005

Supervisory Committee

Dr. Michel Lefebvre, Supervisor
Department of Physics and Astronomy

Dr. Rob McPherson, Supervisor
Department of Physics and Astronomy

Dr. Peter Wan, Outside Member
Department of Chemistry

Dr. Dugan O'Neil, External Examiner
Simon Fraser University

Supervisory Committee

Dr. Michel Lefebvre, Supervisor
Department of Physics and Astronomy

Dr. Rob McPherson, Supervisor
Department of Physics and Astronomy

Dr. Peter Wan, Outside Member
Department of Chemistry

Dr. Dugan O'Neil, External Examiner
Simon Fraser University

Abstract

This thesis outlines the prospects for top quark mass measurement through the Fully Hadronic decay of top-antitop events with the ATLAS detector. Methods with and without b-tagging were explored. Without b-tagging the signal was hidden beneath the QCD multi-jet background and prospects for a mass measurement do not appear to be good. A standard and a pessimistic b-tagging likelihood significance value were explored. The standard value gives a S/B of 0.88 and the more pessimistic value gives a S/B of 0.79. For 1 fb^{-1} a significance of 36.8 and 32.0 can be obtained for the standard and pessimistic scenarios respectively. A selection efficiency of 1.4% and 1.1% can be achieved for the standard and pessimistic values respectively. Assuming a top mass of 174 GeV, a mass peak can clearly be seen for both b-tagging

values. For the standard scenario, a top mass of 168.94 GeV with a statistical error of 0.33 GeV can be extracted. With the pessimistic scenario, the extracted mass is 169.11 GeV with a statistical error of 0.36 GeV. This is the first attempt with fully simulated events and therefore there are possibilities for improvement. This analysis did not include b-jet energy scale correction.

Table of Contents

List of Figures

List of Tables

Acknowledgements

I would like to thank the many people that assisted me with my work for the last two years. First and foremost, my supervisors Professor Michel Lefebvre and Professor Rob McPherson. Learning to code Athena and ROOT is a difficult task and could not have been accomplished without the help of Dr. Rolf Seuster, Gregory King, Tayfun Ince and Dr. Damir Lelas. The samples for this work were kindly generated by a number of people, both within the UVic group, as well as outside. Dr. Rolf Seuster and Frank Berghaus were responsible for the generation of the UVic group. Marion Lambacher and the rest of the LMU group, along with the CSC group, generated the rest. Haley Oxenham was kind enough to ensure that this thesis was consistent with APA standards.

Chapter 1

Introduction

The purpose of physics has always been to explain the world around us. Currently the best method for describing the microscopic world is called particle physics, or more specifically a theory called the Standard Model of particle physics. Particle accelerators and colliders are the basic tools of particle physics, since they allow us to create the particles that we want to study and observe the interactions between them. Detectors are used to study particle collisions and their effect on the surrounding environment. Most collisions produce particles which decay quickly to form ordinary matter. This thesis focuses on the mass measurement of the top quark through a specific decay called the Fully Hadronic decay.

1.1 Particle Physics

In particle physics the fundamental laws that control the make-up of matter and the physical universe are expressed by excitations of quantized fields obeying symmetries. Each type of excitation in each field can be associated with a classical particle. Particle physics studies the basic elements of matter and the forces acting between them. The most successful theory of particle physics is the Standard Model of particle physics [1]. The Standard Model of particle physics is a theory which describes how three of the four known fundamental forces interact to make up all known matter. The Standard Model is based on three relativistic quantum field theories: Quantum Electrodynamics (QED), Quantum Flavour Dynamics (QFD) and Quantum Chromodynamics (QCD). The Standard Model falls short of being a complete theory of fundamental interactions, primarily because it does not include gravity.

The Standard Model consists of two classes of particles, fermions and bosons. QED describes the electromagnetic interactions of charged fermions. QFD explains the weak interactions that govern the flavor change of fermions. QED and QFD are unified to form the theory of electroweak interactions. Fermions are particles of half odd integer spin and form ordinary matter. The fermions are split into two groups, the quarks and the leptons. This thesis focuses on the most massive quark, the top quark. QCD governs the strong interaction between coloured particles which acts to bind quarks into colour singlet hadrons such as protons and neutrons. Leptons are uncoloured so they do not feel the strong force. Bosons have integer spin and are often dubbed the force carriers of the Standard Model because they are responsible for the different interactions associated with force. The photon is the mediator for electro-magnetism, the W's and the Z are responsible for the Weak force while the gluons are responsible for the strong force. The last boson of the Standard Model is the Higgs boson which is a by-product of the mechanism responsible for how particles acquire mass. It was added to explain electroweak symmetry breaking. This is not to be confused with the graviton which is the force carrier for gravity in some theories beyond the Standard Model. The Higgs boson is a product of particles acquiring mass whereas the graviton mediates how particles interact through gravity. The Higgs boson is the only particle in the Standard Model that has not been observed.

As can be seen in Fig. 1.1 the fermions are broken up into 3 generations (I, II and III) while the bosons are each arranged by their known symmetry. This makes for 25 particles which are individually named in the Standard Model. Furthermore, each quark can come in 3 colours and each fermion has an associated anti-particle. Most particles decay quite quickly so they do not exist in the matter we interact with in everyday life. To produce particles like the top we need to build large particle colliders.

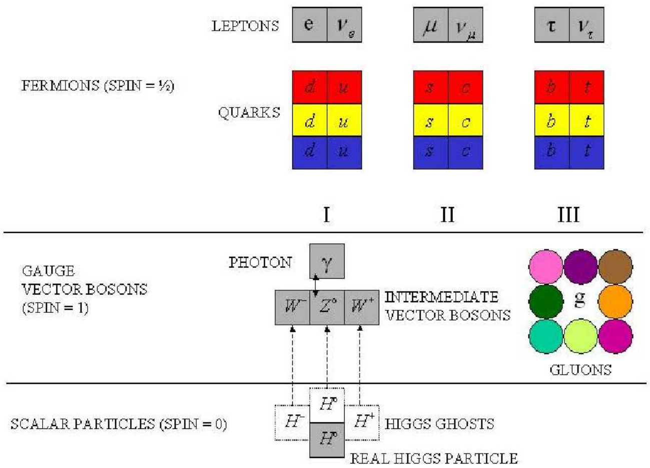

Fig. 1.1: 37 Standard Model particles are shown with some of their interactions and symmetries. There are an additional 24 anti-particles from the fermions.

1.2 The LHC at CERN

At the time of writing this thesis, the European Organization for Nuclear Research (CERN) was within one year of completing the world's highest energy particle collider, the Large Hadron Collider (LHC). It is a circular accelerator with a circumference of 27 km, built approximately 100 m underground straddling the Switzerland-France border. The LHC will produce proton-proton collisions at a centre of mass energy of 14 TeV [2]. This energy will be enough to test the Standard Model with searches for the Higgs. Furthermore, improvements on current measurements are expected to be made. Since it could be found that the Standard Model is incorrect, tests for extensions to the Standard Model have undergone thorough investigation.

The LHC is being built in the tunnel that formerly held the Large Electron-Positron collider (LEP). The LHC has many advantages over LEP, such as higher energy and luminosity. There will be less loss of energy due to synchrotron radiation because of the larger mass of the proton [3]. Although the higher energy of the LHC will allow for the ability to probe down to a smaller length, it has some disadvantages to LEP. According to the Standard Model electrons are elementary whereas protons are made of partons such as quarks and gluons. Because of this, the electron-positron interaction is much cleaner than the proton-proton interaction. Any two of the proton's partons can have a hard interaction while the remaining partons are still involved in the process. The partons not involved in the hard process are known as the underlying event and can significantly complicate the measurement. Additionally, since the partons have varying momentum, the center of mass energy can be different from event to event.

The beam is not continuous but broken into bunches of about 1.15×10^{11} protons spaced by 25 ns at high luminosity, 10^{34} cm^{-2}s^{-1}. The bunch harmonic number is the time taken to encircle the ring divided by the bunch spacing, in other words it is the maximum number of bunches that could possibly be in the ring. The bunch harmonic number is 3564 but the number of bunches in the ring averages to 2808 because there are empty bunches. The event rate, R, by which a given interaction will occur is given by,

$$R = L\sigma, \tag{1.1}$$

where σ is the cross section for the process and L is the Luminosity of the interaction. The cross section for a minimum-bias event* of 70 mb implies that there will be about 0.7×10^9 interactions per second at high luminosity. This corresponds to about 22.2 interaction per bunch crossing. Other proton-proton collisions that are in the same or previous bunch crossings but detected at the same time are referred to as pileup. Along with the underlying event, pileup is a major experimental difficulty because it is difficult to separate this from the interesting "hard" process which is to be measured.

1.2.1 ATLAS

The LHC beams can be collided at one of four locations where detectors are being installed. The detectors at these points are named ATLAS, CMS, LHCb and ALICE. The detector this thesis is based upon is A Toroidal LHC ApparatuS (ATLAS). The ATLAS collaboration was formed in 1992 and the ATLAS detector will begin taking data in 2008.

ATLAS is a multi-purpose detector that is capable of accurately measuring all known particles, except of course neutrinos. Since the ATLAS detector is nearly hermetic† it can give some idea of where there may be neutrinos by conservation of momentum. This can only be done in the transverse (radial) direction due to resolution effects and is complicated by many other affects. There will be significant

*Minimum-bias is defined as non-single-diffractive inelastic.
†Hermetic is defined as the ability to detect particles in all directions from interaction point.

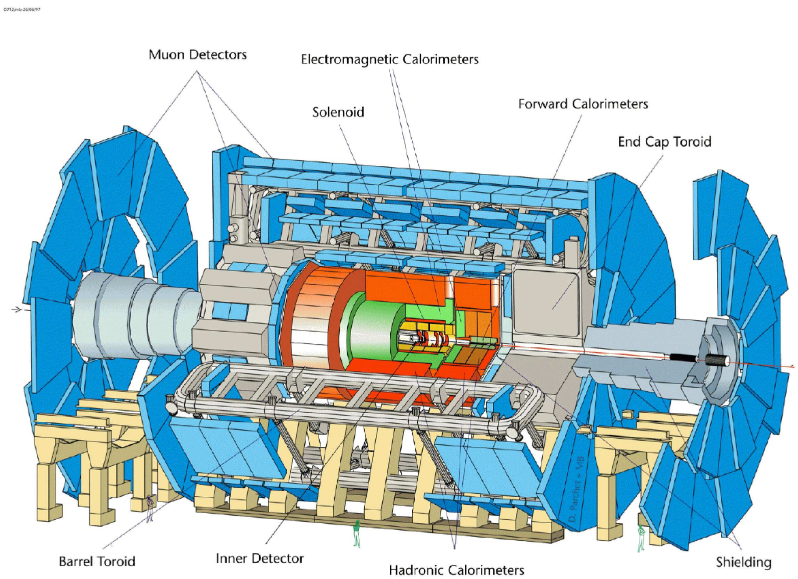

Fig. 1.2: The different sections of the ATLAS detector. The detector is about 44 m in length, 22 m in height and weighs 7000 tons [4].

missing energy along the beam axis in both directions. In order to accomplish this the ATLAS detector has several different types of subsystems, as illustrated in Fig. 1.2. The inner tracker measures the trajectories and momenta of charged particles to find the decay vertexes. The momentum is measured via the radius of curvature of the path taken by the particle in the magnetic field created by the central solenoid. The electromagnetic calorimetry systems measure the energy and incoming direction of electrons, photons, pions and other charged particles, except muons. The hadronic calorimeters measure the energy and position of hadronic particles. The differing amounts of energy deposited in each calorimeter help greatly in particle identification, as displayed in Fig. 1.3. The muon spectrometer identifies muons and determines their momentum.

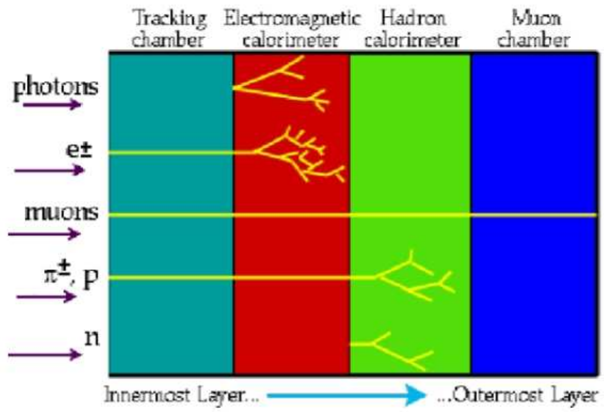

Fig. 1.3: A pictorial diagram which represents the various detector layers and how they can be used for particle identification.[5]

The coordinate system of the ATLAS detector is set with a right handed Cartesian coordinate system, with the y-axis up, the x-axis toward the center of the ring and the z axis along the beam. The origin of the azimuthal angle, $\phi = 0$, corresponds to the positive x-axis and increases clock-wise looking into the positive z direction. The polar angle is measured from the positive z-axis. Pseudorapidity, η, is defined by

$$\eta = -\ln\left(\tan\frac{\theta}{2}\right). \quad (1.2)$$

Transverse momentum, p_T , is defined as the momentum perpendicular to the LHC beam axis. ATLAS calorimeters are segmented in η and ϕ, as well as in depth. There are four depth samplings in the EM calorimeter and three or four depth samplings in the hadronic calorimeter.

With 0.7×10^9 interactions per second there is far too much data to record every event. A complicated trigger system is set up to trigger on events which are of interest. The trigger will have to reject nearly all events in order to reduce the 40 MHz (25 ns bunch spacing) down to a manageable 100 Hz. Further details on the ATLAS detector can be found in the *ATLAS Detector and Physics Performance Technical Design Report* [6].

1.3 Jets & Hadronic Showers

Because this thesis relies on the identification and measurement of jets and hadronic showers, they will briefly be discussed here. Quarks and gluons cannot propagate freely because they are not colour singlets. In most cases they quickly hadronize into colour singlet hadrons, such as pions. When a quark or gluon is produced with high energy, these hadrons are boosted into a collimated spray. This collimated spray is known as a jet. It is by detecting this jet that the 4-momentum of the original quark or gluon can be inferred.

High energy hadrons initiate particle showers when they come into contact with matter such as the ATLAS detector. Because of the complexity of hadronic showers, there are several models. One of these is the spallation model, where hadronic showers are seen as the interactions between high momentum hadrons and a nucleon within the nuclei of the calorimeter material. These interactions can cause the nucleon to be ejected from the nucleus which can then travel and interact with other nuclei. Nuclei which undergo interactions are often left in an excited state. They then emit photons or other particles in order to reach their ground state. A hadronic shower can therefore contain many different types of particles. This causes a hadronic shower to contain both hadronic and electromagnetic energy. The complexity of this process means that two hadronic showers originating from the same type of particle in the same calorimeter can be quite different.

The average length a neutron can travel in a material, the nuclear interaction length, can be quantified as

$$\lambda_I \approx \frac{35A^{1/3}}{\rho}\text{cm}, \tag{1.3}$$

where A is the atomic mass of the particle and ρ is the density in g/cm^3. Since the ejected particle will in general carry less momentum than the particle causing their ejection, the shower will broaden and die out. The depth in which 95% of the showers energy has be thermalized can been calulated as:

$$L(95\%) \approx 2.5[0.54\ln(E) + 0.4]\lambda_I \tag{1.4}$$

where E is the energy in GeV [7]. For more information on calorimetry see [8], [9] and [10].

Chapter 2

Top Quark Properties

When the top quark was discovered in 1995 at Fermilab [11],[12] it completed the predicted generation structure of the Standard Model. The top quark is distinguished from other quarks by its significantly larger mass, about 35 times larger than the next heaviest, the bottom quark. Its large mass is predominantly responsible for many of the properties that separate it from the other quarks. It is the only known quark which decays before hadronization, and does so almost exclusively through the single mode $t \to Wb$.

2.1 Top Quantum Numbers

The Standard Model states that the top quark is a spin-1/2, charge-2/3 fermion which transforms as a colour triplet under the group SU(3) of the strong interaction and as the weak-isospin partner of the bottom quark. None of these quantum numbers have been experimentally confirmed although there is a large amount of indirect evidence to support these assignments. Recent Tevatron RunII data is giving direct evidence for a positive charge assignment. Analysis of electroweak observables in Z^o decays [13] require the existence of a weak isospin, T_3=1/2, charge-2/3 fermion, with a mass in the range of the top mass measurements. The existence of an isospin partner for the b-quark is strongly motivated by arguments of theoretical consistency and symmetry of the Standard Model. Absence of flavor changing neutral current in B-meson decays [14] also gives weight to the need for a partner to the bottom. Direct measurements of these properties are expected to be made at the LHC.

The mass of the top quark is purely a theoretical notion since it can not be observed as a free particle. Therefore the concept adapted for its definition is important when stating what is meant by a measurement of the top quark mass. Historically the top quark mass has been experimentally defined as the position of the peak in the invariant mass distribution of its decay products. This closely corresponds to the pole mass of the top quark, defined as the real part of the pole from the top quark propagator [15]. The current world average for the mass of the top quark found by direct observation is 174.2 $\pm$ 3.3 GeV [16]. It is interesting to note that the top quark's mass is suspiciously close to the electroweak symmetry breaking scale. This suspicion has prompted many theoretical investigations into whether the top quark could play other special roles than what is proposed by the Standard Model.

2.2 Top Production

At hadron colliders, such as the LHC, top quarks are produced mainly in $t\bar{t}$ pairs. At the LHC, the hard process $gg \to t\bar{t}$ comprises 87% of this production cross section, while $q\bar{q} \to t\bar{t}$ comprises the remaining 13%. The next-to-leading order cross section calculation with next-to-next-to-leading soft-gluon corrections for $t\bar{t}$ production is $\sigma(t\bar{t}) = 872.8 \pm 15$ pb [17]. At low luminosity, corresponding to an integrated luminosity of 10 fb^{-1}, more than 8.7 million $t\bar{t}$ pairs will be produced per year. This abundance has caused the LHC to be often referred to as a top factory. The electroweak single top production processes, whose cross sections are in total approximately one third of those for the $t\bar{t}$ production, are important but unrelated to this thesis.

2.3 Top Decays

The top quark decay is mediated by the electroweak interaction. Since flavor changing neutral currents are forbidden in the Standard Model due to the GIM mechanism [18], the decays of the top quark involving the Z or γ bosons are highly suppressed and can only occur in higher order diagrams; therefore, the top quark decay vertex must involve a W boson. The three final states are therefore: $t \to Wb$, $t \to Ws$ and $t \to Wd$.

In quantum mechanics, the lifetime (τ) of a particle is related to its natural width, Γ, through the relationship $\tau = \hbar/\Gamma$. As discussed shortly, the full width, $\Gamma(t \to X)$, can be approximated by the partial width of $\Gamma(t \to Wb)$. Assuming $M_W = M_b = 0$, the lowest order calculation of the partial width yields:

$$\Gamma_o(t \to Wb) = \frac{G_F M_t^2 |V_{tb}|^2}{8\pi\sqrt{2}} = 1.76 \text{ GeV}, \tag{2.1}$$

where G_F is the Fermi constant and V_{tb} is the Cabibbo-Kobayashi-Maskawa (CKM) matrix element linking top and bottom quarks. It is important to note that in this approximation the width is proportional to the top mass squared, M_t^2. The high mass of the top quark is predominantly responsible for its large width. More sophisticated calculations add negative corrections to give 1.42 GeV with theoretical uncertainties less than about 1%. Putting this into $\tau = \hbar/\Gamma$ we get a lifetime of aprroximately $\tau = 4 \times 10^{-25}$ s. This is about an order of magnitude less than the characteristic time for Quantum Cromo-Dynamics (QCD) effects to take place. This implies that the top quark will decay well before it has a chance to form a hadron. This is phenomenologically important because it implies that the decay products retain much more of the quark's information than if it had been effected by QCD before decay.

As illustrated in Eq. (2.1) the first order partial width of charged current top decays are proportional to the square of the corresponding CKM matrix element. Assuming the Standard Model, the relevant CKM matrix elements have the following constraints [19]:

$$0.0048 < |V_{td}| < 0.014, \tag{2.2}$$

$$0.037 < |V_{ts}| < 0.043, \tag{2.3}$$

$$0.9990 < |V_{tb}| < 0.9992. \tag{2.4}$$

Therefore, the $t \to Wb$ decay completely dominates with a predicted branching ratio, $BR(t \to Wb)$, greater than 99.8%. So from a $t\bar{t}$ pair we almost always end up with two bottoms and two W's. It is important to note that before decay the W is on shell so that its mass will corresponds to the normal measured mass.

The $t\bar{t}$ decay chains can be classified according to how the W boson decays. A W can decay leptonically to a lepton and its associated neutrino or hadronically to a pair of quark weak isospin partners. The quarks form jets and most jets are nearly indistinguishable, so there is no way to tell which type of quark initiated the jet. The decay channels of a $t\bar{t}$ pair studied at ATLAS are the Semileptonic, Fully Hadronic and Di-leptonic channels. In the Semileptonic channel, one of the W bosons decays leptonically ($W \to l\nu$) and the other one hadronically ($W \to jj$) giving a final state topology of $t\bar{t} \to (jjb)(l\nu b)$. Defining l to be only electrons and muons, the branching ratio is BR ≈ 2 x 0.2132 x 0.676 ≈ 28.8%*. In the Di-leptonic channel, both W bosons decay leptonically giving a branching ratio of BR ≈ 0.2132 x 0.2132 ≈ 4.5%. In the Fully Hadronic channel, both W bosons decay hadronically leaving a final state topology of $t\bar{t} \rightarrow (jjb)(jjb)$. The branching ratio for the Fully Hadronic channel is the largest of the three being BR ≈ 0.676 x 0.676 ≈ 45.7%. You may have noticed that these do not add up to 100%; this is because τ leptons are excluded and only electrons and muons were considered. The various τ decay chains are illustrated along with the others in Fig. 2.1.

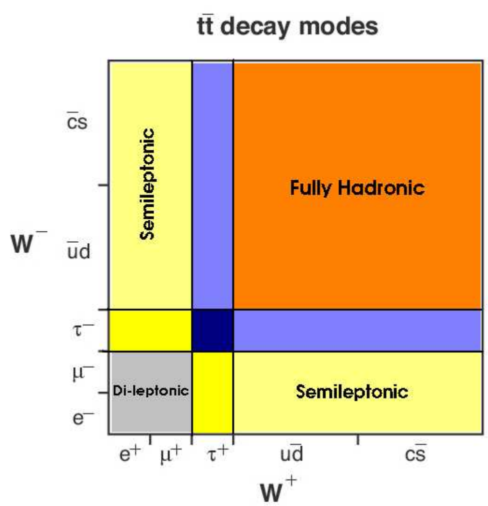

Fig. 2.1: The various branching ratios of the $t\bar{t}$ decay chain. The area represents the ratio of the cross section taken by each chain.

*Values taken from [16]

Chapter 3

Motivation For the Study of the Top Quark

An accurate determination of the top quark mass is important for modern physics for several reasons. Being a fundamental parameter of the Standard Model, it is clear that it should be measured as accurately as possible. The interplay between the fundamental parameters of the Standard Model provides constraints which can be used as consistency checks. For example a more accurate measurement of the top mass would further constrain the predicted mass of the W boson within the Standard Model. Furthermore, a high level of accuracy on the top mass value* is also desirable within the Minimal Supersymmetric Standard Model (MSSM) framework [20]. In

*For example improving the accuracy down to $\Delta m_t \approx 1$ GeV which is what is expected from RunII of the Tevatron.

the MSSM such an accuracy would put constraints on the parameters of the scalar top (stop) sector and would therefore allow sensitive tests of the model by comparing predictions with direct observations.

3.1 Precision Electroweak Fits

The Standard Model has held up to dozens of tests over the last few decades [19]. No discrepancies between theory and experiment have been found up to the current energy scale of a few hundred GeV. Of course this could soon change when the LHC comes on line to give access to the TeV mass scale. Greater precision in experiment will allow for lower theoretical uncertainties in predictions.

The top quark plays a central role in the predictions for many Standard Model observables by contributing to their radiative corrections. In many calculations for radiative corrections there appears the term for one-loop top quark corrections,

$$\Delta\rho = \frac{3G_F M_t^2}{8\sqrt{2}\pi^2}. \tag{3.1}$$

The uncertainty on the Fermi constant G_F is negligible relative to that on the top mass, M_t. As an example of these radiative corrections, consider the theoretical calculation of the W boson mass:

$$M_W^2 = \frac{\pi\alpha}{\sqrt{2}G_F \sin^2\theta_W}\frac{1}{1-\Delta r}, \tag{3.2}$$

where α is the fine structure constant, θ_W is the Weinberg angle and Δr contains the radiative corrections approximately by:

$$\Delta r \approx \Delta r_o - \frac{\Delta\rho}{\tan^2\theta_W}. \tag{3.3}$$

The scalar term Δr_o is a result of the energy scale dependent renormalization flow (running) of α. Δr_o and θ_W are both known to a precision of 0.2% so that the uncertanty in Δr is dominated by $\Delta\rho$. The uncertainty on the top quark mass is currently about an order of magnitude larger than the other uncertanties in the calculation of Δr and moreover, it contributes quadrically. There are several other quantities such as $\sin\theta_W$ and the ratio of b-hadron production, R_b, that are calculated using $\Delta\rho$. Thus, accurate measurement of the top quark mass constrains other measurable quantities in the Standard Model and therefore tests consistency.

Δr contains logarithmic corrections due to Higgs mass loops. Accurate measurements of the top mass in tandem with the W mass can also put constraints on the Higgs mass using Eq. (3.2). Currently the accuracies on the measurements of M_t and M_W are enough to set bounds but these could be improved. Because of the logarithmic dependence of this term, the accuracies would have to be greatly improved for a moderate improvement in the Higgs mass constraint.

3.2 The Top Quark Beyond the Standard Model

Because of the range of possibilities for physics beyond the Standard Model, there are many ways that top quark could play a special role. A brief overview will be given here, but for a more complete analysis refer to [21].

The Standard Model is an effective theory; meaning that it is known to only be accurate in a certain energy range. The Standard Model must break down before gravity effects are needed to be accounted for at the Plank scale †. Since the Standard Model has only been tested up to a few hundred GeV, it is expected that it will break down long before the Plank scale. Most current models anticipate some new physics around the TeV scale.

Since the mass of the top quark is only about a factor of 6 less than this new physics scale it is expected to be more related to this new physics than any other Standard Model particle. The top's Yukawa coupling, y_t, to the Higgs field is approximately equal to unity:

$$y_t = \sqrt{2}\frac{M_t}{\nu} \approx 1, \tag{3.4}$$

†The Plank scale $\approx 10^{19}$ GeV.

where ν is the vacuum expectation value of the Higgs field which is know from properties of the weak interaction to be approximately 246 GeV. Similarly to the mass being close to electroweak symmetry breaking scale and the width being just enough for the top to decay before hadronization, this is just a numerical argument and is not true evidence for anything. All three could simply be coincidence, but they have made many theorists suspicious that the top quark mass could be a more fundamental parameter of nature. This suggests that no matter which theory replaces the Standard Model it will be important to have an accurate measurement of the top mass.

The most well known theory for extensions to the Standard Model is Supersymmetry, SUSY. SUSY extends the Standard Model by adding a bosonic state for every known fermionic state and vice versa for known bosonic states [22]. Just as each particle has an anti-particle each particle would have at least one SUSY partner. There are several variations of SUSY. The ATLAS Supersymmetry Working Group is studying signatures for discovering SUSY as well as methods for studying the properties of SUSY if it is discovered. The group has emphasized detailed studies of particular points in parameter space for the Minimal Supergravity (mSUGRA), Gauge Mediated SUSY Breaking (GMSB) and Anomaly Mediated SUSY Breaking (AMSB) models as well as for models with R-parity violation [23].

SUSY has several features that make it the favourable candidate to extend the Standard Model. SUSY elegantly solves the gauge hierarchy problem since the fermion and boson partners cancel each other's divergent corrections to the Higgs boson mass. The two equal and opposite loop corrections are shown in Fig. 3.1. The lightest Supersymmetric particle should be only weakly interacting and therefore is a good candidate for dark matter. It also predicts the unification of the gauge coupling constants at the GUT scale and is required in the only consistent theory of quantum gravity to date, super-string theory.

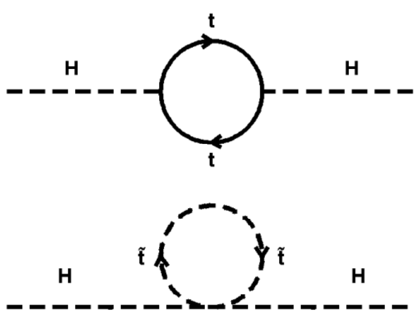

Fig. 3.1: The Feynman diagrams for the cancellation of the Higgs boson quadratic mass renormalization between fermionic top quark loop and scalar stop squark loops in SUSY [21].

The top quark plays an important role in SUSY models. Similarly to how the top quark is important to the radiative corrections in Standard Model electroweak observables, the radiative corrections from SUSY particles to electroweak observable are dominated by loops involving the top quark and its scalar partners, the stop squarks ($\tilde{t}$). The Higgs sector is particularly sensitive to these corrections. If we consider the most simplistic version of SUSY, the Minimum Supersymmetric Standard Model (MSSM), there are 5 physical Higgs bosons. The one loop correction to the lightest MSSM Higgs boson mass, M_h, is proportional to [14]:

$$\Delta M_h^2 \approx G_F M_t^4 \log\left(\frac{M_{\tilde{t}_1} M_{\tilde{t}_2}}{M_t^2}\right), \tag{3.5}$$

where $M_{\tilde{t}_1}$ and $M_{\tilde{t}_2}$ are the masses of the lightest and heaviest stop squarks respectively. Clearly these corrections depend quartically on M_t, so the same conclusions can be stated for SUSY as the Standard Model. Top quark mass uncertainties will be a limiting factor in the self consistency checks and predicting unknown parameters.

There are other less popular theories to replace the Standard Model above the TeV scale. Many of these theories involve dynamical breaking of the electroweak symmetry [24]. These Strong Dynamics models do not include an elementary Higgs boson but rather give mass to the particles by introducing a new strong gauge interaction that produces condensates of fermions which act as Higgs bosons. These models have fallen out of favour since Tevatron has discovered no evidence for this new force. In the models known as Topcolor the new gauge interaction acts only on the third family of quarks causing the condensate to be made of top quarks [25]. Such models could be discovered by looking for peaks in the $t\bar{t}$ invariant mass spectrum.

3.3 The Fully Hadronic Channel

The Fully Hadronic channel is not likely to give the most precise measurement of the mass of the top quark. Despite this is it is still an important measurement to be made and it has been done so at CDF [26], [27]. D0 was also able to isolate this signal and make a cross section measurement [28]. ATLAS work on this channel was first published in the *ATLAS Detector and Physics Performance Technical Design Report* [6] citing a simple analysis [29] and has continued up to the present [30].

The Fully Hadronic channel is sensitive to the sources of systematic error in different ways than the other two channels. This is mainly due to the fact that the important backgrounds are different for each channel. This systematic difference implies that this measurement could be used as a consistency check between the methods used. Also, it will add to the combined measurement of the top quark mass.

The development of this signal extraction and measurement process is not limited to top mass measurement. If a top mass is assumed, it is an extra constraint which can be used for isolation of this signal. Of course you could no longer use this to measure the top mass but the cross section is still unbiased. A $t\bar{t}$ resonance exists in SUSY, Topcolor and several other models. It is possible in some models that the best way to measure this is in the Fully Hadronic channel.

Another use is the possibility to measure the Higgs mass in the $(t\bar{t})(H) \rightarrow (Wb)(W\bar{b})(b\bar{b}) \rightarrow (jjb)(jj\bar{b})(b\bar{b})$ chain [31]. The major problem for this is that the normal ATLAS trigger would not trigger on these events preferentially to the large QCD background. Since there is no obvious characteristic which distinguishes this from the multi-jet background there will be nothing to trigger on. The proposed strategy is to develop a distributed trigger based on a complicated selection algorithm somewhat similar to the kinematic method discussed in this thesis. This trigger would transport all multi-jet events directly to the Tier-1 centers via a high-speed network. It is proposed to take a total bandwidth requirement of about 10 Gb/s which means that it is possible to process all multi-jet events by allocation about 1% of the offline analysis capacity to the reconstruciton of $t\bar{t}$ Higgs candidate events.

Methods for background elimination could be useful to future studies done on similar samples. In the MSSM with R-parity violation and non-unified gaugino masses, there is a significant amount of parameter space in which the Higgs decays to a pair of unstable neutralinos, each of which subsequently decays to a quark and a squark. The two squarks then decay to two quark jets leaving a final state of six jets [32]. This is virtually the same decay chain as $t\bar{t}$ Fully Hadronic except for the interchange of the tops with neutralinos and the W's with squarks. The $t\bar{t}$ Fully Hadronic will in this case be a background to this process.

3.4 Analysis Objectives

The main goal of this thesis is to investigate the best possible method to measure the top mass in the Fully Hadronic channel. Two things must be taken into account when defining a measure on "best" for this circumstance. The first is time; it would be nice to have results as soon as possible. Not all resources are available when the

ATLAS detector is first turned on, so if our analysis is dependent on one of these resources then there will be a delay. b-tagging will take some time to set up, so if it is required then there will be a delay. The second measure on “best” is the top mass resolution which is related to the number of events. The term “statistics” refers to the statistical error present when low numbers of events are involved analysis. For all methods the resolution will improve when a greater amount of data is available because the statistical error will be reduced. Since statistical uncertanty will improve with time, a compromise will have to be reached. We want results as quickly after initial collisions as possible, but the longer the LHC runs the better our statistics and b-tagging abilities are. The reality of limited or no b-tagging for initial data led us to consider the possibility of an analysis which does not require b-tagging.

Chapter 4

ATLAS Monte Carlo Samples

Since this thesis is in preparation for the LHC there is no true data. Event simulation is a very important and sophisticated method for testing what we expect to see in the ATLAS detector. Precise theory is only known for the parton interactions so it is important to model extrapolations and detector response correctly. What is generated is of course model dependent. All samples generated for this analysis are within the Standard Model. Since the parameters of the Standard Model are not fixed by theory they must be entered into the generator. These are parameters like the top and W mass which are taken as 174 GeV and 80.419 GeV respectively. The Width of the W, Γ_W, is generated as 2.12 GeV.

Monte Carlo algorithms are a commonly used class of computational algorithms for simulating the behaviour of various physical and mathematical systems. It is stochastic, or nondeterministic, in some manner by the use of pseudo-random numbers. Each Monte Carlo event takes a random point in the parameter space for the process.

In order to produce Monte Carlo events on which to perform analysis, a full chain of steps needs to be taken to produce Analysis Object Data (AOD) as shown in Fig. 4.1. Because of the time this process takes, especially the simulation stage, it is unlikely that most users will produce events themselves, but will rely on centrally produced official samples. However, initial test samples needed to be created locally for this work.

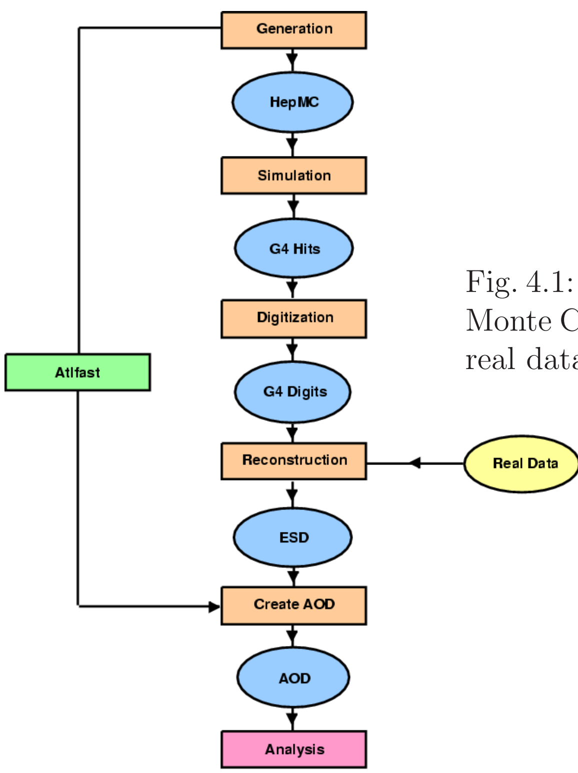

Fig. 4.1: Schematic representation of the Full Chain Monte Carlo production. Both GEANT4 digits and real data are reconstructed as ESDs. [33]

Full Chain simulation can be sped up by using ATLFast which provides a fast simulation of the whole chain by taking the generated events and smearing their values to produce Analysis Object Data directly. This loss of sophistication and therefore accuracy, is often well worth the amount of time it saves. The general framework for all ATLAS analyses is Athena.

4.1 Monte Carlo Generation

Generation refers to the production of particle 4-vectors for specified physics processes. There are many event generators available. The most common in ATLAS are PYTHIA [34] and HERWIG [35] which have only leading order matrix elements. PYTHIA and HERWIG are multi-purpose event generators designed to simulate all stages of a p-p collision and output the 4-vectors of all the particles at each stage. HERWIG needs the addition of JIMMY [36] to model underlying event. Newer event generators such as ALPGEN [37] and MC@NLO [38] run at next to leading order but are limited to specific interactions. MC@NLO is a HERWIG based package for combining a Monte Carlo event generator with Next-to-Leading-Order calculations of rates for QCD processes. Hadronization from HERWIG is often used in conjunction with these generators.

As summarized in Fig. 4.2, generation of an event in a Monte Carlo p-p collision is done in several steps. First,two partons (one from each proton) collide to produce the hard subprocess which then forms two final state particles. This is referred to as a 2 to 2 process because the 2 initial state particles collide to form 2 final state particles. The initial sate particles can radiate gluons before the interaction; this is called initial state radiation (ISR). Similarly the final state particles can produce final state radiation (FSR) in the parton cascade. The parton cascade is the process where quickly decaying particles such as the top decay. The next step is for the final state particles to undergo hadronization to form jets of hadrons. These hadrons are mostly unstable and therefore undergo further decays. The remaining partons from the proton no longer form a colour singlet and must therefore decay to form the underlying event. Pile-up can also now be added at this stage by overlaying minimum bias events.

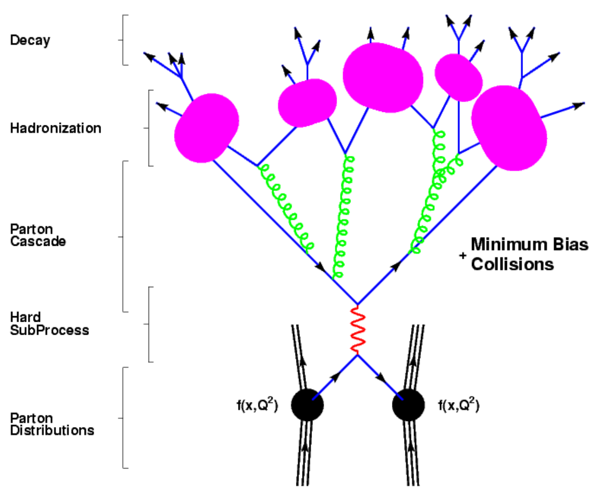

Fig. 4.2: Schematic diagram of the generation for a Monte Carlo event [39].

4.2 Simulation and Digitization

Simulation is the process whereby generated events are passed through a GEANT4 [40] simulation of the ATLAS detector to produce GEANT4 Hits. GEANT4 Hits are a record of where each particle traversed the detector and how much energy was deposited. The path of the decay chain is followed though the simulated ATLAS detector. This must be done in discrete step sizes but these are chosen small enough that only one material is contained within each step. The understanding of how each particle interacts with each type of material is calculated empirically and validated by precision beam tests. A hit is recorded for each step that occurred in material that could detect and record the information related to this particle. For example, a neutrino will not be recorded in a calorimeter. Also, no particle will record a hit if the step is done in dead material such as the detector's supporting structure; although, this may be required for a detector performance study unrelated to a physical measurement that will be made in the real detector.

Digitization is the process whereby the GEANT4 hits from the simulation are subjected to the response of the detector to produce digits, such as times and voltages. The hits produced from the simulation step are digitized in 25 ns bins and the effects from the detector and its electronics such as light attenuation and electronic noise are applied to resemble actual detector response. These are stored in the Raw Data Object (RDO) while adding an identifier. As can be seen in Fig. 4.1, RDOs contain the same information as the byte stream which comes from the detector, but they are not in the same format. Although there will be truth information in the Monte Carlo events stating how each event was generated. A realistic analysis will not use truth information in the measurement because it will not be available with real data.

4.3 Reconstruction

The reconstruction stage combines the output of all the detectors to determine the important quantities. These could be simple quantities such as the 4-vector of a particle or more complicated objects, such as those related to b-tagging. Reconstruction is the stage where the RDO is reconstructed into tracks and energy deposits as Event Summary Data (ESD). The ESD consist of sufficient information to re-run parts of the reconstruction, such as track refitting and jet calibration. For most analyses the information available in an RDO or ESD is excessive. The Analysis Object Data (AOD) is a summary of the reconstructed ESD. An AOD consists of a reduced size output of physics quantities from the reconstruction that should suffice for most kinds of analysis work. Separate tailor-made streams of AODs are foreseen for different needs of the physics community. This analysis was done on standard AODs.

4.3.1 Jets

There are several ways to define and build jets so it is important to specify exactly which method was used. Clustering of calorimeter cells is the first step in defining a jet. The cell is the smallest calorimeter reconstruction object. All ATLAS calorimeters together provide 187652 cells. Each of which provides the raw reconstructed energy in MeV. Clusters of calorimeter cells in the jet context are called particles and are the building blocks of jets. There are two types of particles commonly used in ATLAS reconstruction; topological clusters and towers. A tower is a group of cells in a fixed $\Delta\eta \times \Delta\phi$ grid over some or all samplings. Towers contain the sum of cell energies and the center of the grid as members. A cluster is a group of cells formed around a seed cell. Clusters are the main reconstruction object for calorimetry. Topological clusters have variable borders based on the significance of the adjacent cells. These contain many data members based on weighted cell members for energy, position and shape.

There are pros and cons for both the towers and topological (topo) clusters. Towers have a fixed size of 0.1×0.1 in $\Delta\eta \times \Delta\phi$ [*], and all cells are used in towers. All the energy is in some particle and because of this they do not provide noise or pile-up suppression. Additionally, a small particle shower on the edge of a tower will not be contained in one tower. Topo clusters on the other hand provide efficient noise and

[*] 0.1 for the $\Delta\phi$ is defined as $2\,\pi/64$.

pile-up suppression on average but may be sensitive to pile-up on event by event. Topo clusters are more likely to not split energy deposits from a hadron, which gives validity to calling these objects "particles". The drawback of topo clusters is that they typically have detector region dependent size.

Jet finding algorithms are run on particles to build the jets. There are several methods for defining rigorously what a jet is. This ambiguity has caused the development of several different jet finding algorithms. As a standard, ATLAS uses a seeded cone algorithm with split and merge functions available. The cone algorithm takes all the particles within a $\Delta R^{\dagger}$ cone of either 0.7 or 0.4. A seed cone is placed in all particles passing an E_T cut of 1 or 2 GeV. There is also the k_T algorithm which could give better results because of its ease to compare with theory. In the k_T algorithm (FastKt) nearness in relative transverse momentum is used. Cluster particles are grouped in order of increasing relative transverse momentum. In order to terminate cluster merging a maximum is required on the D parameter, the standard values are 0.6 and 0.4. The difference between Cone and k_T is illustrated in Fig. 4.3. Typically an E_T minimum of 7 or 10 GeV is required of the final jets.

Energy Scale Calibration is important so that the energy of the jet accurately represents the energy of the particle which initiated the jet. All cells are initially calibrated to EM scale. EM scale is a calibration such that the energy readout of

$^{\dagger}\Delta R = \sqrt{\Delta\phi^2 + \Delta\eta^2}$.

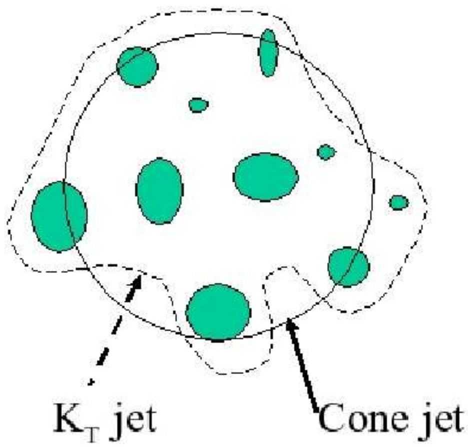

Fig. 4.3: Pictorial diagram representing the difference between the Cone and k_T algorithms.

the detector will give the energy of the EM particle which interacts with it. In other words, if a 100 GeV electron entered the calorimeter it would record 100 GeV. The detectors are calibrated with EM particle beams. Since hadronic showers are different from EM showers, the calorimeter would not in general record the correct energy of the hadronic particle. If a shower is known to be hadronic a calibration must be applied in order to adjust the scale appropriately. There are two hadronic scale calibration approaches in jet reconstruction. Local Hadron Calibration is to calibrate topo clusters to hadronic scale independent of any jet algorithm, then jets are formed from calibrated topo clusters. The standard jet calibration uses towers or topo clusters on EM-scale as input to jet algorithms. A calibration function is then derived from Monte Carlo. If it is possible to match a truth particle jet with each reconstructed jet, a fit to a cell-level calibration function based on energy density to all matched jet pairs can then be derived.

When analyzing an AOD, choosing a jet finding algorithm comes down to selecting which ParticleJetContainer is to be used. The name contains the algorithm, the size of the jet in the algorithm and the type of clustering used, in that order. At the closing of this thesis there are several possibilities: Cone4TopoParticleJets, Cone4TowerParticleJets, Cone7TopoParticleJets, Cone7TowerParticleJets, Kt4TopoParticleJets, Kt4TowerParticleJets, Kt6TopoParticleJets and Kt6TowerParticleJets, each produced with their own weights. In the future, it is expected that all the topo jets will have Local Hadronic Calibration. The reason Local Hadronic Calibrated topo clusters are desired is because this is the best way to factorize the detector response correction from the jet corrections to particle jet scale, and to physics dependent scale.

A new and promising algorithm boldly called the Optimal Jet Finder (OJF) may be the best choice for this analysis [41]. In this algorithm, a bias toward how many jets are to be found can be made. For this analysis, jet merging and jets not from the hard process has increased the complexity and therefore degraded results. If the OJF was to constrain many of these events to have 6 hard jets then it is possible that we would have a Fully Hadronic sample with a higher percentage of the 6 jets reconstructed well. This algorithm was not ready in time for use on this analysis.

This thesis used the cone tower algorithm with R = 0.4, or Cone4TowerParticleJets. This was decided upon initially as it is the choice suggested by the top group.

4.3.2 b-tagging Objects

Another important object of reconstruction is the b-tagging likelihood significance. A jet is not given a simple yes or no tag, since it is very difficult to discern if the jet originated from a bottom quark. b-tagging is most often expressed as a weight value which is the likelihood of the jet to be a bottom. There are several of these associated with each jet. They represent different methods to determine if a jet originated from a bottom quark. Extensive literature on b-tagging can be found in [42], but a brief summary will be given here. b-quarks quickly form B-mesons after production so b-tagging is not looking for b-quarks so much as B-mesons. Due to the relatively long life-time of the b-flavoured mesons, the decay will on average take place a few mm from the primary vertex. A possible signature in the detector could thus be a secondary vertex which can be reconstructed. In addition, characteristics of b-jets such as jet-kinematics, semileptonic decays of the B-mesons, and impact parameters can be used to separate b-flavoured jets from jets with lighter flavors.

It is possible to reconstruct secondary vertexes in the b-flavoured jets. There are several ways of seeding the secondary vertexes and assigning tracks to the vertexes. One way is to fit vertexes with all pairs of tracks, retaining the fit with the highest probability and fitting the remaining tracks of the jet to this vertex. All tracks below a certain fit probability will be rejected. This approach is implemented in the build-up algorithm. Another approach is to start with all tracks in the jet, fit a vertex, and reject tracks below a certain fixed fit probability. This has been implemented in the tear-down algorithm. Most of the b-tagging studies have been done from the decay of the Higgs boson [6] but some results have been verified for tops and show no significant difference.

4.4 Samples for this work

The Monte Carlo simulation for this analysis was generated by three separate groups. The initial samples were generated locally by the University of Victoria (UVic) group. For these samples, matching and detector simulation was done with ATLFast on Athena 12.0.31. Hadronization was done with HERWIG 6.510 and the underlying event was modelled was with Jimmy 4.2. Several samples were created for initial tests. A $t\bar{t}$ sample with all decays of the $t\bar{t}$ was generated on MC@NLO 3.1.0. QCD multi-jet backgrounds and W+njet background were created with AlpGen 2.0.6. Different samples of QCD multi-jet backgrounds were generated with 2,3,4 and 5 hard particles along with a 6 jet inclusive sample (denoted 6++). The W+njet samples were generated with a hadronically decaying W for n= 2,3 and 4++.

After this initial analysis, it became clear that the W + njets background was not large enough to be considered farther. Also, that a QCD multi-jet sample was needed with enhanced b-jet probabilities if b-tagging was to be explored. Official samples were then obtained from two separate groups. The official ATLAS samples for $t\bar{t}$ were obtained from the CSC group. These samples have been labelled as CSC5204‡ and CSC5200§ by the group so these names will be kept. The CSC5204 sample is the sample containing the Fully Hadronic decay of the $t\bar{t}$ pair and the CSC5200 sample contains all other $t\bar{t}$ decays. The matrix element was done by MC@NLO with the rest of the generation being done by HERWIG. Documentation for this generation can be found in [43].

The QCD multi-jet background was generated and validated by the ATLAS group of Ludwig-Maximillians-Universitat (LMU) in Munchen [44]. The UVic group then obtained their 4-vectors and reconstructed the samples in Athena 12.0.6 using ATL-Fast. The samples were normal QCD multi-jets with 3,4,5 and 6++ jets as well as QCDB samples with b-jet enhancement generated with 4, 5 and 6++ jets. The QCDB jets samples occur the regular QCD samples but are very rare and most likely not in the right proportion. These enhanced samples were generated with b-jets to assure that there would be enough passing selection. Many of the samples mentioned above were found to be eliminated by the analysis method relatively easily. This does not imply that they would not be a background only that we do not have enough events to make a statement about them. Luckily the samples which were expected to form the largest backgrounds had enough events. For this reason only the samples CSC5204, CSC5200, LMUQCD6j, LMUQCD6jB, LMUQCD5j and LMUQCD5jB will

‡More specifically trig1_misal1_mc12.005204.TTbar_FullHad_McAtNlo_Jimmy.recon.v12000601

§More specifically trig1_misal1_mc12.005200.T1_McAtNlo_Jimmy.recon.v12000601 have results presented for them. The samples are listed in Table 4.1.

Table 4.1: The samples generated for this analysis along with their cross sections and if they were used in the final analysis. The 6 jet samples are inclusive but lack the "++" for brevity.

Sample	Type	Group	Cross Section	Used
ttbar	All $t\bar{t}$ Decays	UVic	987.654 pb	No
W+4++ Jets	W with 4 Jets	UVic	266.241 pb	No
W+3 Jets	W with 3 Jets	UVic	968.263 pb	No
QCD2 Jets	Multi-jet	UVic	91458400 pb	No
QCD3 Jets	Multi-jet	UVic	6108940 pb	No
QCD4 Jets	Multi-jet	UVic	986113 pb	No
QCD5 Jets	Multi-jet	UVic	173852 pb	No
QCD6 Jets	Multi-jet	UVic	34334.6 pb	No
CSC5204	Fully Hadronic $t\bar{t}$	CSC	372 pb	Yes
CSC5200	Leptonic $t\bar{t}$	CSC	461 pb	Yes
LMUQCD3j	Multi-jet	LMU	4766000 pb	No
LMUQCD4j	Multi-jet	LMU	480000 pb	No
LMUQCD5j	Multi-jet	LMU	48000 pb	Yes
LMUQCD6j	Multi-jet	LMU	26000 pb	Yes
LMUQCD4jB	Multi-jet with bs	LMU	69000 pb	No
LMUQCD5jB	Multi-jet with bs	LMU	16000 pb	Yes
LMUQCD6jB	Multi-jet with bs	LMU	4000 pb	Yes

The uncertainties on the predictions of the cross sections at LHC energies are considerable due to error in the calculation of higher order strong diagrams. Much of this error results from the large strong coupling constant, α_S. The uncertainty along with different generation cuts and MLM matching criteria are the cause of the difference in QCD cross sections. The $t\bar{t}$ cross sections are taken to be the theoretical values. The Top Group has chosen to use a standardized $t\bar{t}$ cross section of 833 pb along with 372 pb for the Fully Hadronic channel.

4.4.1 Monte Carlo Truth and Signal

Most Monte Carlo generation samples include a truth particle container¶. The truth particles are the particles as they are created in the generation stage. Only the truth of the jets will be discussed here in detail as the truth for leptons and other single particles are well defined. It should also be noted that there are Truth Jets which are jets formed from jet algorithms being run on the particles in the truth container. These will not be used in this analysis. The truth particles of interest are the 6 partons corresponding to the (jjb)(jjb) final state.

A truth container has all the particles that exist in each event in all their states of generation. For example there is more than one top (or anti-top) in the truth container because of the several phases that the top goes through before decay due to the Monte Carlo generation method. These are of course the same top recorded at different times. We want the 6 particles that correspond to the quarks forming jets. It was decided that the choice would be to take them in the form in which they are first produced. This means the truth bottom quarks are defined to be the bottoms which are produced in the top decay not any of the following states it forms before or during hadronization. Similarly the light quarks are taken as the two quarks that are produced by the W decay. It should be noted that a photon or gluon can be produced at the same time in this decay.

¶In this case a TruthParticleContainer named SpclMC.

The Truth Matched jets are defined as the 6 jets which are matched one to one with the truth particles. Since a jet's 4-vector is not, in general, the same as the truth particle which it came from, the word "matched" needs to be defined rigorously. A jet is matched to a particle if it is the closest jet within $\Delta R = 0.4$; so any jet which has a cone containing the original particle is a candidate. The closest jet is then taken to be the one matched to the particle. If two particles are matched to the same jet then the event is considered unmatchable.

What may be surprising is that many events in the CSC5204 sample are not able to be matched. The subset of the CSC5204 sample in which all six of the quarks have been reconstructed as six distinct jets is quite small. Refer to Table 4.2 to see that is this also dependent upon the jet finding algorithm. Although Cone4TowerParticleJets have the lowest matching efficiency this does not imply that they should not be used for this analysis. It could actually imply the opposite because other jet algorithms may be splitting jets more frequently.

Table 4.2: The truth matching efficiencies for the smaller sized jet finders available.

Algorithm	Cone4Tower	Cone4Topo	kT4Tower	kT4Topo	kT6Tower	kT6Topo
# Events	71,914	71,914	71,914	71,914	71,914	71,914
# Truth Matched	20,368	28,342	39,062	37,196	31,073	29,972
% Truth Matched	28.3	39.4	54.3	51.7	43.2	41.7
% light Quarks	84.5	88.9	91.9	91.2	91.1	91.6
% Bottom Quarks	89.1	92.7	95.0	94.5	94.2	93.9
% W's	69.6	77.6	84.1	82.7	80.9	80.0
% Top Quarks	59.3	69.3	78.3	76.6	73.1	72.1

An important cause of this small truth matching efficiency is that higher momentum can cause these 6 particles to be reconstructed as a fewer number of jets. If the

W is boosted relative to the detector the two quarks could be reconstructed as one jet because they will not have time to separate before they hit the detector. Both of the initial particles would then be matched to the same jet. In a more extreme case a highly boosted top can be reconstructed as one jet. If a jet radiates a hard gluon then it may not be matched to the truth because of the change in direction. This change in direction is also likely to cause the jet to have a much different energy from its originating particle.

An analysis tries to find the correct values from within a signal sample. It is therefore important to be able to define when the analysis produces the correct result. Some of the events in the CSC5204 sample do not have 6 jets which reconstruct to two tops; so, it would be expected that not all of the CSC5204 sample will be signal and therefore is background. The signal is the six jet Fully Hadronic decay of $t\bar{t}$. This is the subset of the Fully Hadronic sample, CSC5204, in which a match to the truth can be found. The signal cross section will be the CSC5204 cross section scaled by the truth matching efficiency. This implies that the signal cross section is in some way jet finder dependent. This is not surprising since the term jet is in the definition of our signal as the 6-jet Fully Hadronic decay of $t\bar{t}$.

Chapter 5

Analysis of Simulated Events

The Athena framework was used for this analysis, although much of the preliminary work was done in ROOT on n-tuples created in Athena. The algorithm used has been adapted from the AnalysisSkeleton package [45]. As the name implies, this class is an analysis skeleton created such that the user can implement his/her analysis by using it as a template.

The analysis can be broken into several sections, which are comprised of different types of selection cuts, a combinatorial algorithm and a kinematic fitting method. The analysis is summarized in Table 5.2. Selection cuts, or cuts, are ways by which you extract signal when mixed with the background. In both Monte Carlo and the real experiment, samples of event candidates are given. In Monte Carlo, specific samples are generated and in the experiment, events are chosen by the trigger. If a variable has a range in which it is more likely to be signal than background this can be exploited to improve the ratio of signal to background. The selection cuts in this analysis proceed in the standard hard cut fashion where those which are not in the specified range are excluded from any further analysis. This is in contrast to other methods such as decision trees, where cuts give specified weights toward a probability. Most cuts are dependent on some value which can be adjusted to optimize the signal passing relative to background.

As discussed in the section 4.4, a Signal sample as well as several background samples were produced. Clearly the background is undesirable and we would like to eliminate as much of it a possible. These are the CSC5200, LMUQCD6j, LMUQCD6jB, LMUQCD5j and the LMUQCD5jB samples. The part of the CSC5204 sample which can not be matched to truth is also background. Since this is matching and jet finder dependent, some events would be labelled as signal under different conditions. It would be undesirable to call the whole CSC5204 sample the signal because for all signal events you should be able to have a correct assignment of the jets to the 6 jet event topology.

In a signal event in which all six quarks are reconstructed as different jets, it is still very unlikely that there will only be six jets in the event. Other jets can come from initial state radiation (ISR) or final state radiation (FSR). This can happen for either quarks or gluons and is illustrated in Fig. 5.1 for quark ISR. If FSR does not form a distinct jet then it is considered part of the kinematics of the jet. Quarks (most often b-quarks) can fragment in several different ways causing some to be reconstructed as two jets. There is also the matter of pile-up and underlying event which was discussed in previous sections. All of the jets in a signal event which are not matched one to one with a truth particle will be referred to as *other jets* for lack of a better term.

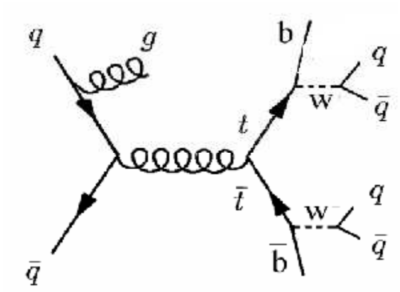

Fig. 5.1: An example of typical initial state radiation.

This method includes combinatorial permutations of the jets to make jet assignment hypotheses. This implies that, in a signal event with only the six correct jets there will be many assignment hypotheses which are incorrect. As will be shown later, such an event will have 90 possible combinations with only one being correct. These 89 incorrect combinations would also need to be considered as background and therefore need to be eliminated by the analysis. The problem is exacerbated when *other jets* are added because each of these *other jets* could be hypothesized to be a correct jet. So any jet assignment in the signal which is not the correct 6 1-1 matched jets will be called combinatorial background.

Each selection cut should remove a higher fraction of the background than of the signal. It is also important to keep enough statistics in the signal to make a measurement. Sufficient background events are needed to pass the analysis to have a measure on the size and importance of each background. The strength of the selection cuts are then limited by the number of events in the available samples. Experimentally this corresponds to how many events pass after some decided upon luminosity. It was decided that 1 fb^{-1} was a reasonable amount in which to calibrate our analysis.

5.1 Jet Selection Criteria

The first set of selection criteria will be referred to as *jet cuts* because they remove jets from further consideration. From an experimental perspective they are the criteria for selecting jets within an event. In the Monte Carlo there is a jet container which contains the jets simulated for each event. We would like to eliminate jets that do not correspond one to one with one of the six quarks. The best way to distinguish these *other jets* is that on average they will have lower p_T. We therefore want to exclude jets which have p_T lower than some optimized value. Dedicated research [46] shows that a cut value should be set to the p_T of the lower p_T jet from each W. This cut is labelled *jet cut* 1 and is adjusted to cut all jets with p_T lower than 30 GeV. Later cuts are more restrictive on the specific jets according to hypothesis.

It is also necessary to restrict the pseudorapidity, η, region such that $|\eta| < 3$. This, the second *jet cut*, was chosen for us by the performance of the calorimetry systems and the greater amount of *other jets* close to the beam pipe. It is an ATLAS Top Working Group convention to analyze tops in this region essentially as a result of these reasons. Since conventions are important for comparison to other work, this convention was followed.

5.2 Event Selection Criteria

The second set of selection criteria will be referred to as *event cuts* because they can cut a whole event from further analysis. Refer to Table 5.2 for an overview of the analysis. After the jets that did not pass the *jet cuts* have been removed from each event, there will be some number of jets in each event. The kinematic fit used later requires 6 jets for reconstruction so this is also necessary for the analysis. The first *event cut* is therefore on the number of jets in the event. Clearly if the event has less than six jets then it will not be suitable for later analysis.

Since the signal is a subset of the Fully Hadronic decay of $t\bar{t}$, an event of this type will not have any parton cascade level leptons; refer to Fig. 4.2. Of course there will be several leptons that come out in hadronization and decay; but, since these do not come from decays of high mass particles, their energy should be much lower than that of parton cascade level leptons. The exception would be leptonic decays of the b-quarks but these should be contained within the b-jets; therefore, the 2^{nd} *event cut* is to cut if there is an isolated electron with high p_T. Isolated is defined by the amount of energy around the electron* being less than a threshold. This threshold is given by a linear functional dependence on the energy and is standardized by the Top Working Group. The 3^{rd} *event cut* is the same, but for muons. Similar to the leptons, there should also be no neutrinos. Since the ATLAS detector will be unable to detect neutrinos, events with neutrinos will be identified by those with a large missing transverse energy (MET). Neutrinos are clearly not the only source of MET but it is a strong indicator of neutrinos. The 4^{th} *event cut* is then a cut on high missing transverse energy.

Event cuts 2 through 4 were optimized using the CSC5200 sample compared to the Truth Matched sample. Recall that the CSC5200 sample contains the decays of the $t\bar{t}$ which have leptons. The CSC5200 sample is a reasonably large background and gives a good measure on these selection variables because of the presence of parton cascade level leptons. The values were chosen such that virtually none of the Truth Matched jets were rejected, while still rejecting a majority of the CSC5200 sample. The values were set to be 80 GeV for electrons, 50 GeV for muons and 60 GeV for missing transverse energy.

At this point we hope to have eliminated many of the undesirable events from both our signal and background. We would now like to permute these jets into all possible hypotheses of jet combinations. If we take N to be the number of jets remaining in

*Specifically parameter(ElectronParameters::etcone).

the event after the *jet cuts*, then the combinatorics is the ways in which we can assign these N jets to the 6 quarks in unique ways such that none are repeated. Clearly this number grows quickly with N so we want to remove events which still have many jets. This is *event cut* 5. Another reason a cut such as this will help is that if there are many high p_T jets then the $t\bar{t}$ is more likely not be reconstructed as 6 jets or that it was not $t\bar{t} \rightarrow (jjb)(jjb)$ at all.

Event cut 5 has been the source of a fair bit of debate since it is unclear what is the best way to deal with too many jets in an event. When looking in truth it was found that events with higher remaining jet multiplicity were less likely to be truth matched. The value of 8 was chosen to be the maximum number of jets allowed in an event. Any event with more than 8 jets after the event selection cuts will be cut from further analysis. This could also have been done in a different way as to not remove any events at all. It is possible to take only the highest p_T X jets of the N and ignore the others. X would likely be set to 8 as well. It was unclear if this more complicated method would be of any merit, so it was not done.

5.3 Combinatorics

A combinatorial algorithm produces all the possibly correct hypotheses for each event. For this analysis it is done as follows. First, the six jets for a hypothesis of the $t\bar{t}$

event are chosen giving $\binom{N}{6}$† combinations. Next, the three quarks that will be one of our tops are chosen from these six. It is very important to note that you only need to choose half as many as you would initially assume because while choosing one top as three quarks you are indirectly specifying the other because it is the remaining three. This amounts to $\frac{1}{2}\binom{6}{3}$ additional combinations. We then want to specify the W from within each top, ie $\binom{3}{2}$. Note that is equivalent to specifying the b, ie $\binom{3}{1}$, since $\binom{3}{2} = \binom{3}{1}$. We want to do this for both tops so this adds an additional $\binom{3}{2}^2$. Note that the assignment of the 2 light quarks in the W need not be permuted as the analysis does not distinguish between the two. The total number of combinations for N jets is then

$$\binom{N}{6}\frac{1}{2}\binom{6}{3}\binom{3}{2}^2. \tag{5.1}$$

It can be clearly seen from Table 5.1 why a maximum on N was set in *Event cut* 5.

Table 5.1: The number of possible jet assignment hypotheses for N jets.

N	6	7	8	9	10	11	12
Hypotheses	90	630	2520	7560	18900	41580	83160

It is important to note that since we are only interested in the top mass there are only $\binom{N}{6}\frac{1}{2}\binom{6}{3}$ combinations with different top mass hypotheses. There are $\binom{3}{2}^2 = 9$

† $\binom{N}{M} \equiv \frac{N!}{M!(N-M)!}$

hypotheses with the same top masses before the kinematic fitter. These will all be altered by the kinematic fitter so the final top mass will be different. The kinematic fitter will be discussed more thoroughly later. There are also many hypotheses with one top assignment correct. This implies that many of the signal events with the wrong combinations will have at least one top mass hypothesis with the correct scale.

5.4 Hypothesis Selection Criteria

After the jet combinatorics has been taken into account we are left with many hypotheses for the jet assignments for each event. We can now make *hypothesis cuts* to rule out hypotheses which are unlikely to be correct assignments or are background.

As mentioned above, the two light quarks from the W should be treated differently based on p_T. On average one will be high in p_T while the other low in p_T because of their decay directions relative to the rest frame of the W. The b jets will in general have a higher p_T than the softer light quark jets but the harder light quark jets will have a similar shape. These distributions are illustrated in Fig. 5.2. QCD multi-jet background jets are on average much softer. *Jet cut* 1 was adjusted to the softer of the two light quark jets p_T and is an overall minimum. We can therefore distinguish Fully Hadronic $t\bar{t}$ events with the correct hypothesis as having these four jets with a high p_T. The first *hypothesis cut* is to cut if either b-jet hypothesis has p_T less than 45 GeV. The second *hypothesis cut* will be to require at least one of the light quarks from each W to have p_T above 50 GeV.

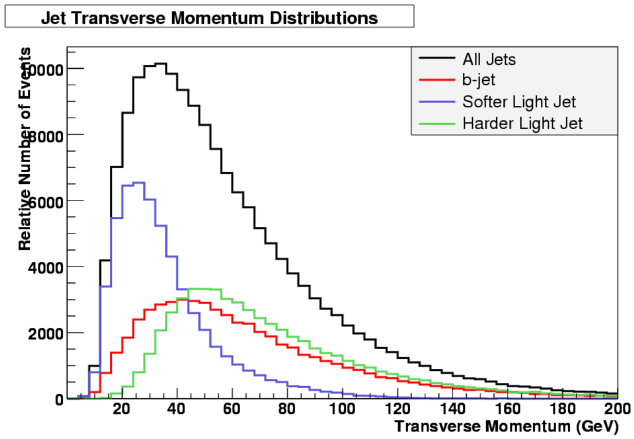

Fig. 5.2: The p_T distributions for the correct assignment of the truth matched jets of the Truth Matched sample.

As discussed previously, the two light quarks coming from the W are often so close together that they are reconstructed as one jet. If they are not, we can use this to our advantage. We cut a hypothesis if the ΔR separation between the two light quarks from the W is higher than 2.3. This is *hypothesis cut* 3 and the related variables are depicted in Fig 5.3. Similarly, *hypothesis cut* 4 is the same thing but between the W and b. The 4-vector of the W is taken to be the sum of the 4-vectors of the two light quarks. A hypothesis is cut if the ΔR separation between the W and b is greater than 2.3.

The invariant mass of the $t\bar{t}$ system clearly cannot be below two times the top mass. Also, the QCD background will in general reconstruct a higher $t\bar{t}$ invariant mass than the signal. We therefore make the fifth *hypothesis cut* to eliminate all events where the $t\bar{t}$ system's invariant mass is outside the window bounded by some

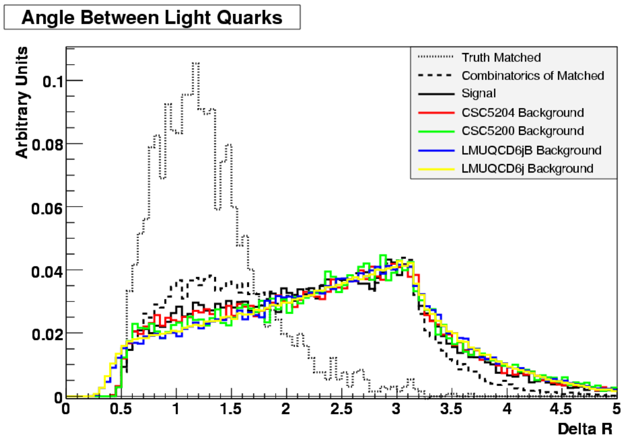

Fig. 5.3: The distributions for the ΔR angle between the hypothesized light quark jets.

set values. The lower value is clearly going to be set to be about twice the top mass and the higher value will be optimized against background. The lower value was taken to be 300 GeV to ensure that the mass was not biased. If the lower value was put to exactly twice the expected top mass value then it would not be able to be found to be less. The higher value was taken to be 800 GeV.

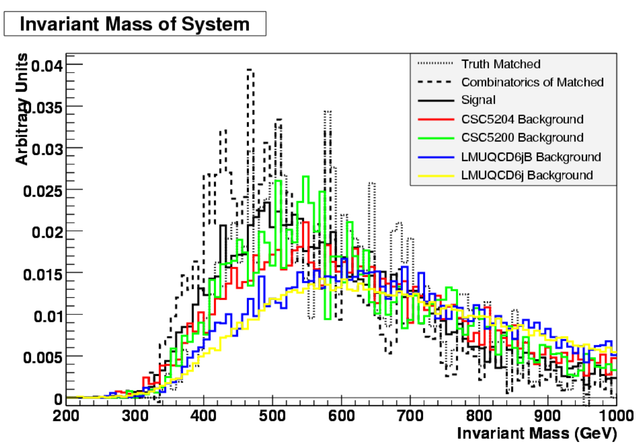

Fig. 5.4: The systems invariant mass of the $t\bar{t}$ hypotheses for the various samples.

The values for the *hypothesis cuts* 1 through 5 were decided upon in the same method. Histograms for the variables were plotted just before they were cut on for a number of different samples. That is, all analysis and cuts previous to the one being optimized were applied and then the distributions were examined. The different samples were then compared to find an appropriate value by inspection. The samples are as follows. The first is the Truth Matched jets because this will give us a measure on what the true shape should be. The second was the combinatorics of these Truth Matched jets, which is the Truth Matched permuted as discussed in the combinatorics section. This sample contains the correct 6 jets but with only 1 in 90 having the correct assignment. This sample will give us a measure on the shape of a distribution containing the part of the combinatorial background that has no *other jets* in the assignment. The third was the Signal sample because it will contain all the combinatorial background. Comparing the Signal sample to Truth Matched will help us to see how close we are getting to a pure sample in the Signal. The last are the associated histograms for the backgrounds. These are the CSC5204 Background subset, CSC5200 and the various QCD samples. As discussed in the sample section, these were only the QCD 5 and 6++ jet samples because the other backgrounds were too low on statistics for a shape to be seen in the histogram.

The next three *hypothesis cuts* have to do with preparing the events for the kinematic fitter. There will be events that the kinematic fitter will not accept and we can eliminate these to get a more stable analysis. The kinematic fitter constrains the two hypothesized top masses to be close to one another so if the two top masses are excessively different we know that the kinematic fitter will not accept this or give a very poor likelihood. The sixth *hypothesis cut* is then to cut if two top masses differ by more than the set value. *Hypothesis cut* 6 was optimized in the same method as 1 through 5 but kept especially loose because it will be dealt with in the fitter and therefore reflected in the likelihood.

The kinematic fitter also constrains the two hypothesis W masses to be close to the current accepted value of the W mass. These are set to the values used in the generator and will be denoted by the subscript "$_o$". The generator values should match the Particle Data Group values if everything is up to date. We then want to eliminate the hypothesis if the average W mass hypothesis is outside a window around the M_{W_o} specified by the set value X, ie $|\frac{1}{2}(M_{W^+} + M_{W^-}) - M_{W_o}| < X$. The 8^{th} *hypothesis cut* is to do the same but for the top mass. One might argue that this cut will add bias to the process because it is using a top mass value in the measurement of itself. This is of course true but the window taken around the top mass will be so large that this bias will be negligible. *Hypothesis cuts* 7 and 8 are mainly to assure that most hypotheses sent to the fitter are topologically sound and will return a successful fit. The values were chosen such that the truth matched jets would rarely be cut.

5.5 Constrained Kinematic Fit

The basic idea of any kinematic fitter is that we have a set of constraints and a set of values which we want to alter so that the constraints are satisfied as much possible. The output values will in general be different and fulfil the constraints better than the original values. A good kinematic fitter will also output some measure, usually a χ^2, on how well the constraints are satisfied. The constraints for this analysis are that the proposed masses for the W's are "close" to the accepted values and the proposed top masses are close to one another. This is counter-balanced by the constraint that the output jets should be "close" to the input jets. "Close" is defined by the resolutions of the jets and the widths of the particles. If only variations in energy are considered, this can be expressed as the minimization of the function

$$\chi^2 = \sum_{j=1}^{6} \left(\frac{E_j^m - E'}{\sigma_{E_j}} \right)^2 + \left(\frac{M_{W_o} - M'_{W+}}{\Gamma_{W_o}} \right)^2 + \left(\frac{M_{W_o} - M'_{W-}}{\Gamma_{W_o}} \right)^2 + \left(\frac{M'_t - M'_{\bar{t}}}{\sqrt{2}\Gamma_{t_o}} \right)^2 . \tag{5.2}$$

The values which are primed, $'$, denote the values which will be varied in the minimization to be the output values. The E^m values are the measured energy values of the jet assignment hypothesis. The σ_{E_j} are the resolutions of the energy of the jets which will be explained in the following subsection. The primed values are varied until a minimal χ^2 is found then the fit energies, E', are set to be the new jet energies.

The values with the subscript null, $_o$, are once again the values used in the Monte Carlo generator. The top mass was generated as a δ function not a Breit-Wigner. We took $\Gamma_{t_o} = 0.1$ GeV to approximate the delta function. The minimization was done such that the 4-vector varied as the energy scale.

$$E \to E' \implies p^{\mu} = \langle E, p_x, p_y, p_z \rangle \to \left\langle E', \frac{E'}{E} p_x, \frac{E'}{E} p_y, \frac{E'}{E} p_z \right\rangle = p'^{\mu} \tag{5.3}$$

A kinematic fit can be good for two reasons. Not only does the χ^2 give a measure on how much the event kinematically fits the proposed topology but the jets are calibrated. This calibration is due to the constraint which forces the light jet pairs to have an invariant mass close to the W mass. Only the light jets are calibrated by this method.

This basic idea was generalized to include the ability to alter the jet's η and ϕ adding to 18 free parameters. For a number of computational reasons there are cases in which the minimization is not possible. If there are more parameters to minimize, then the possibility of not finding a minimal solution increases. If the angles are taken into account there are 18 free parameters and the number of failed fits is much greater than with only six from the energy. For example, in the truth matched jets sample 56 of the 836 hypotheses failed for the 18 parameter method; but there were no failures for the 6 parameter method. Although the 18 parameter method showed a slight improvement in calibration of the light quarks to the W mass it was not used. In Fig. 5.5 the two different methods are compared. If these shapes are fit to a Gaussian the additional 12 parameters change the σ from 0.92 GeV to 0.62 GeV while they both have a mean, μ, of 80.1 GeV. Before the fit σ=8.76 GeV and μ=77.9 GeV. It was decided that it would be better to have more passing fits than a slight improvement in the fit. Since hypotheses failing the fitting method are removed, it can be thought of as the 9^{th} *hypothesis cut*.

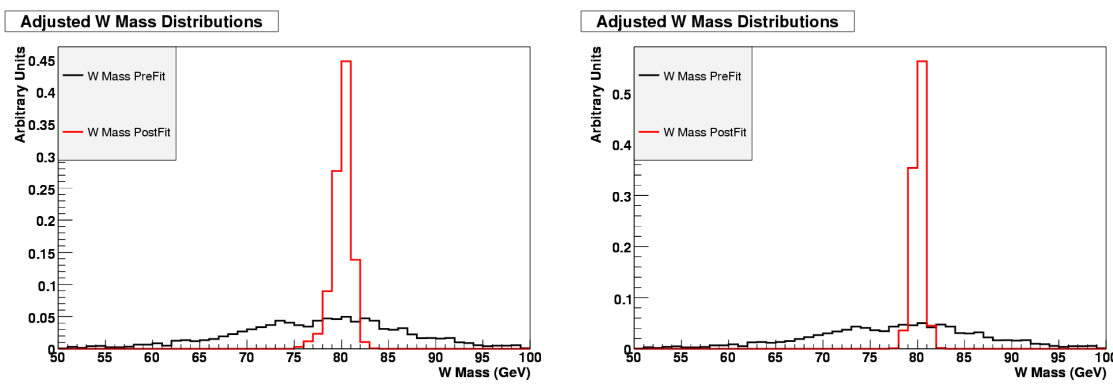

Fig. 5.5: The W mass values for the truth matched jets as adjusted by the kinematic fitter. The left is the plot if only the 6 energy parameters are varied. The right plot is when all 18 free parameter are varied.

The hypotheses which pass *hypothesis cut* 8 are subjected to the kinematic fitter. Since the values of the previous three hypotheses are set appropriately, the kinematic fitter will return adjusted jets and a χ^2 for nearly all hypotheses. We then cut any hypothesis which has a higher χ^2 than the an optimized value of 10; refer to Fig. 5.6.

The first term in Eq. (5.2) is the counter-weight term which restricts the output values from being significantly altered from the input values. The counter-weight term is also an indicator of poor events. This is the 11^{th} *hypothesis cuts* and was optimized to cut if it was greater than 4.5. These two *hypothesis cuts* were optimized in the same method as hypothesis cuts 1 through 5.

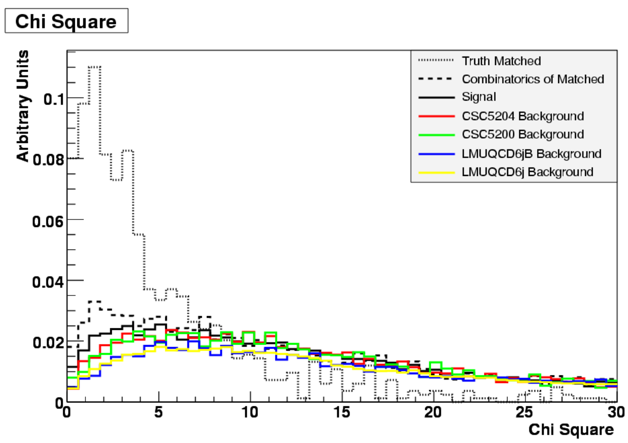

Fig. 5.6: The χ^2 of the hypotheses for the various samples used.

5.5.1 Jet Resolutions

To optimize the abilities of the kinematic fitter, the resolutions of the jets must be known. Let's define in general $\Delta X \equiv X^{Truth} - X^m$ for some quantity X of a jet. X^{Truth} is the value from the Monte Carlo truth particles and X^m is the value of the jet that was matched to each truth particle. Obviously $\Delta X \neq 0$ in general, but ΔX will nearly follow a Gaussian distribution. The mean of the distribution is the bias and the variance of this distribution is defined to be the resolution:

$$\sigma_X \equiv RMS(\Delta X). \tag{5.4}$$

The variances are, in general, functions of energy and pseudorapidity, $\sigma_X(E, \eta)$, but they can also depend on other variables. For this analysis we are only concerned with $\sigma_E(E)$. After some study this was taken to be:

$$\frac{\sigma_E}{E} = \frac{100\%}{\sqrt{E}} \oplus 10\%, \tag{5.5}$$

where E is the energy in GeV. σ_E was shown to have a smaller dependence on η than energy in the range of interest.

5.6 To b-tag or not to b-tag

One of the important questions that was planned to be answered by this thesis is concerning whether b-tagging is necessary for this measurement. b-tagging is the ability to determine if a particular jet came from a b-quark. Clearly this can potentially fix two of the jets assignments and significantly aid the measurement. The question is not whether it will aid, but whether it is needed for a sufficiently precise measurement. It is known that b-tagging will not be available for initial data, so in the interest of obtaining a measurement as quickly as possible, it is important to explore methods without it. The major source for the delay is that we need more than just the calorimeter to implement full b-tagging. A completely calorimeter-based analysis can also be useful in controlling detector systematics. If b-tagging is not needed then it can still be added once it is available; therefore, this can be the 12^{th} and final *hypothesis cut* dependent on the clause that b-tagging is available.

As discussed previously there are several different likelihood significances used for tagging. weight() was used as the tagger for this analysis. This will return the weight of the currently best performing tagger. There are several other possible weights to use. The second most common is lhsig(). Cutting on this weight value gives a certain tagging and mis-tagging efficiency. b-tagging can be added to this analysis as a final hypothesis cut by removing the hypothesis if either hypothesized b-quark has a lower b-tagging weight than a set value. b-tagging will only be available in the region $|\eta| < 2.5$ because that is the range in which tracking will be available. Therefore this has to be an additional part of the b-tagging cut.

Typically in ATLAS analyses, and particularly in fast simulation studies, an overall b-tagging efficiency of 60% (50%) for low (high) luminosity is taken. The mis-tagging inefficiencies for c-jets (other light quark jets) are taken to be 10% (1%). Mis-tagging is when a jet that did not originate from a bottom is tagged as one. Choosing the value of weight() to cut at is additionally complicated by the fact that some of the background was only simulated with ATLFast. This implies that full b-tagging algorithms can not be run on these samples. Instead, ATLFast assigns the quarks either the maximum or minimum values based on the predetermined set of efficiencies mentioned above.

5.6.1 Tagging Efficiencies

The b-tagging efficiencies for fully simulated data depends on the sample. The function weight() returns a value in the range [-30,100]. The standard convention is to say that a weight() above 3 corresponds to the tagging efficiency of 60% with mis-tagging inefficiency of 10% and 1% for c and other light quarks, respectivly. Since this is the efficiency ATLFast has set the backgrounds to, this must be matched for our signal. A weight() cut value of 3 on this sample does not produce these efficiencies. The tagging efficiency was 68% and the dependence on η and p_T can be seen in Fig 5.7.

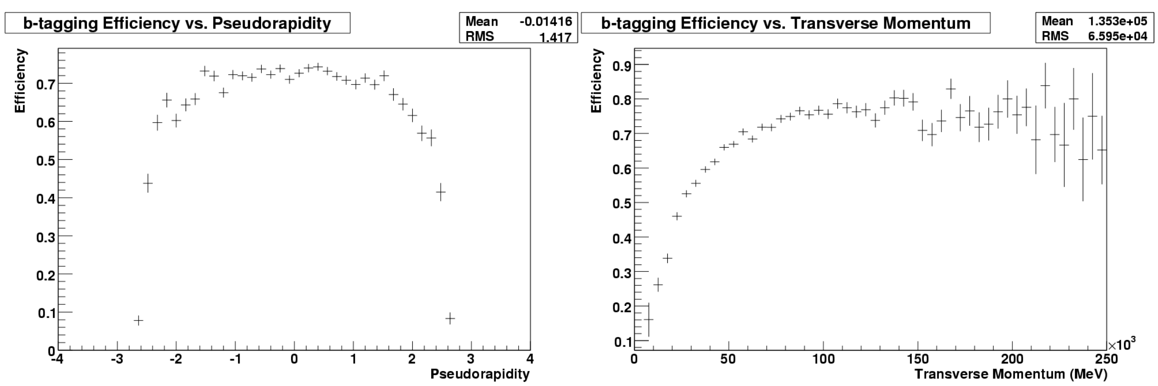

Fig. 5.7: Tagging efficiencies for the Signal sample for a weight() cut of 3. These are dependent on η and p_T.

A new value must be found to ensure that the fully simulated b-tagging efficiency matches the ATLFast b-tagging efficiency. Since it is unlikely that these efficiencies and inefficiencies would be matched at the same value it was chosen to just match the tagging efficiency. A value for the weight() cut will have to be found that matches the ATLFast 60% efficiency. As shown in Fig. 5.8, this can simply be found.

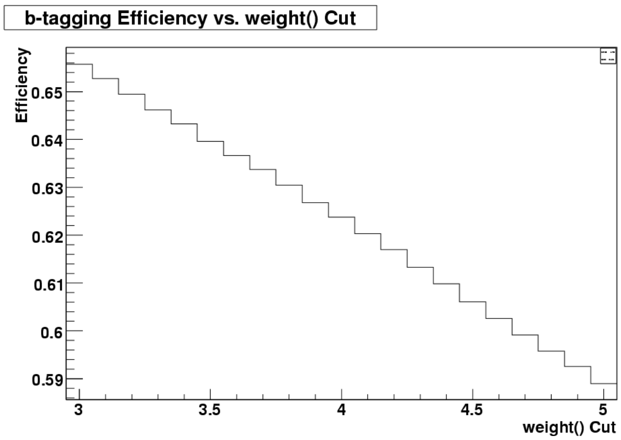

Fig. 5.8: A plot of the efficiency as a function of weigh() cut.

This value was found to be about 4.7 rather than 3[‡]. Choosing this will give a pessimistic scenario for our b-tagging since it is likely that our signal is chosen is such a way to improve the efficiency. This is because the matching algorithm selects well behaved b-jets. As the ΔR in the matching is increased the tagging efficiency decreases. For a weight() cut value of 4.7 the tagging efficiency is 0.5991.

The only way that one could eliminate the problem of what value to use would be with all samples being fully simulated. The value could then be optimized in the standard fashion. Results for both the weight() cut of 3 and 4.7 will be shown. The two different values will be called the standard and pessimistic b-tagging scenarios.

[‡]These values will need to be updated due to changes in the technical aspects of b-tagging and detector modelling.

Fig. 5.9 shows the tagging efficiencies for the pessimistic scenario.

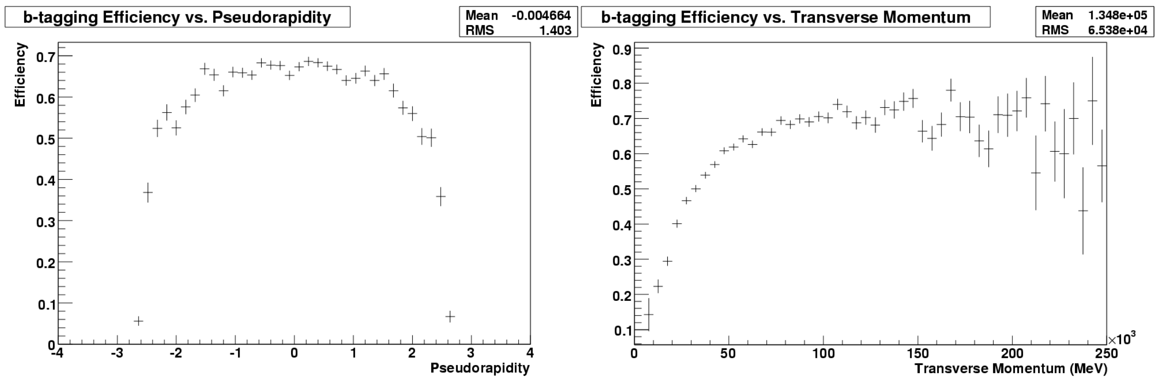

Fig. 5.9: Tagging efficiencies for the Signal sample for a weight() cut of 4.7. These are dependent on η and p_T.

5.7 Other Selection Variables

In such an analysis it is difficult to decide which variables are good for signal discrimination. Many variables show a difference between signal and background, but not all are useful. There are several variables that could have been used but were decided to not be worth the added complexity. Some of these variables will be listed now for completeness and the possibility for assisting future improvements of this analysis.

Previous analyses of this type often had a cut on the top p_T however this was not found to be a useful variable in this analysis. Its usefulness was most likely taken out by other cut variables which were correlated with it. The sum of the top p_T's, $|p_{T_{t_1}}| + |p_{T_{t_2}}|$ was considered, but ultimately dropped. Other variables from the kinematic fitter show some power but were decided against as well. These include:

$$\sum_{W}\left(\frac{E_j^m - E'}{\sigma_{E_j}}\right)^2 + \left(\frac{M_{W_o} - M'_W}{\Gamma_{W_o}}\right)^2, \tag{5.6}$$

$$\left(\frac{M'_t - M'_{\bar{t}}}{\sqrt{2}\Gamma_{t_o}}\right)^2, \tag{5.7}$$

and

$$\sum_{j=1}^{6}\frac{E_j^m - E'}{\sigma_{E_j}}. \tag{5.8}$$

In the *event cuts* there were cuts to veto events with isolated muons and electrons. τ leptons are much more difficult to identify so they were ignored for this analysis. Once they are better understood an analogous veto should be place on τ's.

Recently there was been work done on the possibility of jet algorithms which could distinguish between jets coming from quarks and jets coming from gluons. If this is possible it would make a useful *jet cut* since all the wanted jets come from quarks.

The final values for the cuts are summarized in Table 5.2.

Table 5.2: Overview of the analysis method.

Type	*Cut*	*Value*
Jet 1	Minimum Jet p_T	30 GeV
Jet 2	Minimum Jet η	3
Event 1	Minimum # of Jets	6
Event 2	Maximum Electron p_T	80 GeV
Event 3	Maximum Muon p_T	50 GeV
Event 4	Maximum Missing Transverse Energy	60 GeV
Event 5	Maximum # of Jets	8
Combinatorics		
Hypothesis 1	Minimum b-Jet p_T	45 GeV
Hypothesis 2	Minimum p_T of harder light quark	50 GeV
Hypothesis 3	Maximum $W_{jj}\Delta R$	2.3
Hypothesis 4	Maximum $Wb\Delta R$	2.3
Hypothesis 5	Minimum and Maximum $M_{t\bar{t}}$	300 & 800 GeV
Hypothesis 6	Maximum $\lvert M_t - M_{\bar{t}}\rvert$	45 GeV
Hypothesis 7	Maximum $\lvert\frac{1}{2}(M_{W^+} + M_{W^-}) - M_{W_o}\rvert$	30 GeV
Hypothesis 8	Maximum $\lvert\frac{1}{2}(M_t + M_{\bar{t}}) - M_{t_o}\rvert$	60 GeV
Constrained Kinematic Fit		
Hypothesis 9	Valid Kinematic Fit	-
Hypothesis 10	Maximum χ^2	10
Hypothesis 11	Maximum Counter-weight Term	4.5
Hypothesis 12	Minimum likelihood significance	3 or 4.7

Chapter 6

Results and Discussion

Despite the low number of QCD events passing the selection, much can still be said about the prospects for a measurement. Without b-tagging the prospects for measurement are not good. For each of the two b-tagging values promising results were obtained. The standard value, 3, gives a S/B of 0.88 and the more pessimistic value, 4.7, gives a S/B of 0.79. For 1 fb^{-1}, a significance of 36.8 for the standard scenario and 32.0 for the pessimistic scenario is expected. A selection efficiency of 1.4% and 1.1% can be achieved for the standard and pessimistic values respectively. A top mass peak can clearly be seen with b-tagging. A top mass of 168.94 GeV with a statistical error of 0.33 GeV and 169.11 GeV with a statistical error of 0.36 GeV can be extracted with the standard and pessimistic scenarios respectively.

6.1 Without b-Tagging

As expected, the analysis without b-tagging showed to be very difficult, if at all possible. Table 6.1 shows the cut flow for the various samples. It can be seen that much of the problematic QCD samples have been reduced. Although, due to the high cross sections of these samples they still swamp the signal.

Table 6.1: The cut flow of the number of Monte Carlo events for this analysis without b-tagging.

Sample	Signal	Truth Match	CSC5204 Bkgrnd	CSC5200 Bkgrnd	QCD6jB Bkgrnd	QCD6j Bkgrnd	QCD5jB Bkgrnd	QCD5j Bkgrnd
Cross Section (pb)	105.3	105.3	266.7	461	4000	26000	16000	48000
# of Events	20368	20368	51546	239214	81980	499900	78643	430106
After Event Cut 1	8581	3758	10163	19400	9234	69631	146	1121
After Event Cut 2	8538	3746	10114	17287	9234	69631	146	1121
After Event Cut 3	8474	3718	9980	15594	9234	69631	146	1121
After Event Cut 4	8337	3666	9755	7696	8986	69290	142	1115
After Event Cut 5	8159	3666	9653	7653	8448	64151	142	1115
Efficiency (%)	40.1	18.0	18.7	3.2	10.3	12.8	0.18	0.26
# of Hypotheses	3719160	3666	3252060	2225340	4235760	35484100	17910	138690
After Hypothesis Cut 1	1810310	2034	1679690	1070660	1982590	17003700	7482	62280
After Hypothesis Cut 2	1309660	1320	1288250	780494	1431840	12572500	5306	44686
After Hypothesis Cut 3	316132	1213	287724	160520	297934	2643010	1152	10412
After Hypothesis Cut 4	78581	1049	66333	33097	60468	530946	305	2432
After Hypothesis Cut 5	65496	901	49276	26065	38626	311250	166	1514
After Hypothesis Cut 6	33466	838	21176	10866	13750	107926	76	557
After Hypothesis Cut 7	26061	837	15255	7951	9197	71745	48	373
After Hypothesis Cut 8	25066	836	14325	7417	8077	62746	39	330
After Hypothesis Cut 9	24709	836	14125	7294	7926	61486	37	321
After Hypothesis Cut 10	8821	704	4539	2301	1985	15226	7	71
After Hypothesis Cut 11	4186	518	1917	973	772	6023	2	36
Efficiency (%)	0.11	14.1	0.059	0.044	0.018	0.017	0.011	0.026

Fig. 6.1 shows the top mass hypotheses for the samples of interest. The Truth Matched jets and the truth matched combinatorics (Combinatorics of Matched) are also plotted. Knowing the number of truth matched combinatorics which pass each cut is also instructive as to how we are doing in our analysis. The number of Signal

hypotheses minus the number of Truth Matched hypotheses gives us the number of wrong hypotheses in the Signal sample. The number of Signal hypotheses minus the number of truth matched combinatorics gives the number of wrong hypotheses involving *other jets*. The number of truth match combinatorics hypotheses minus the number of Truth Match hypotheses gives us the number of wrong hypotheses with the correct 6 jets.

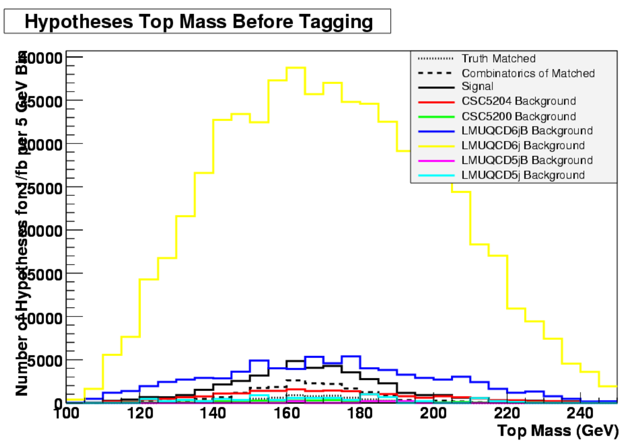

Fig. 6.1: Overlay of the various samples mass hypotheses normalized to 1 fb^{-1}. The samples are in solid lines and those related to truth are dashed.

6.2 With b-Tagging

To add b-tagging to this analysis we simply add the b-tagging cut to the analysis after the last cut; that is, after the counter-weight term likelihood cut. This will keep Table 6.1 given above exactly the same except for the final row. Table 6.2 would replace the last row in Table 6.1. It is important to state that the b-tagging cut is done on the jets as they were before the fitter. Although the adjusted jets are known at this time in the algorithm they are not what should be cut. The b-tagging efficiencies are studied for set p_T and η values. If the jets are then altered by the fitter, their efficiencies still correspond to the previous p_T and η values.

Table 6.2: The cut flow for the final b-tagging cut shown for both values.

Sample	Signal	Truth Match	5204 Bkgrnd	5200 Bkgrnd	QCD6jB Bkgrnd	QCD6j Bkgrnd	QCD5jB Bkgrnd	QCD5j Bkgrnd
Cross Section (pb)	105.3	105.3	266.7	461	4000	26000	16000	48000
# of Events	20368	20368	51546	239214	81980	499900	78643	430106
After standard cut of 3	561	284	152	70	18	11	0	0
Hypotheses for 1 fb^{-1}	2902	1469	786	135	878	572	-	-
After pessimistic cut of 4.7	447	244	128	57	18	11	0	0
Hypotheses for 1 fb^{-1}	2312	1262	662	110	878	572	-	-

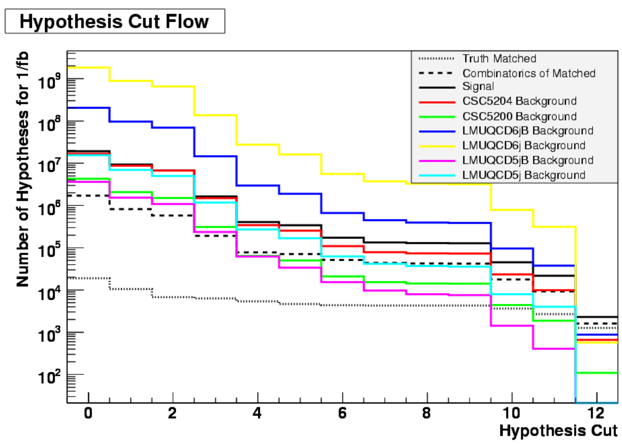

Fig. 6.2: Overlay of the various samples hypothesis cut flow normalized to 1 fb^{-1}. The b-tagging cut is done with weight() > 4.7.

The final *hypothesis cut* flow is illustrated in Fig. 6.2. In total there are 12 *hypothesis cuts* when b-tagging is included. The b-tagging step is the most drastic cut of them all. It can be seen that the Truth Matched sample is relatively flat throughout the analysis. The analysis efficiency can be extracted from the Truth Matched column of Table 6.2. The overall selection efficiency is 1.4% and 1.1% for the standard and pessimistic scenarios respectivly. The standard value gives a S/B of 0.88 and the more pessimistic value gives a S/B of 0.79. For 1 fb^{-1} a significance of 36.8 and 32.0 can be obtained for the standard and pessimistic scenarios respectively.

This method allows for more than one hypothesis per event. This is not necessarily a bad outcome as many of the wrong hypotheses still have one top assignment correct. It is also difficult to distinguish which is the best hypothesis when the truth is not known. It is still promising that there were not very many hypotheses per event as can be seen in Fig 6.3.

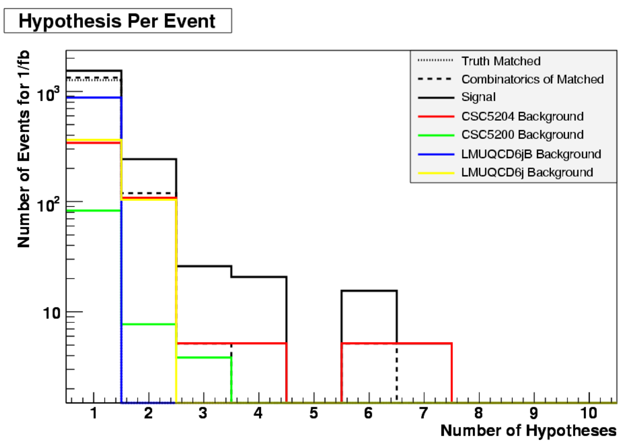

Fig. 6.3: An overlay of the number of hypothesis per event normalized to 1 fb^{-1}. The b-tagging cut is done with weight() $>$ 4.7.

The final top mass plots are given in Fig. 6.4. Compared to Fig. 6.1 it can be seen that the b-tagging gives a huge improvement on the results. It is clear from these plots that the low statistics in the QCD multi-jet backgrounds will be a problem. With infinitesimal bin widths and infinite statistics all the curves in Fig. 6.4 should be smooth.

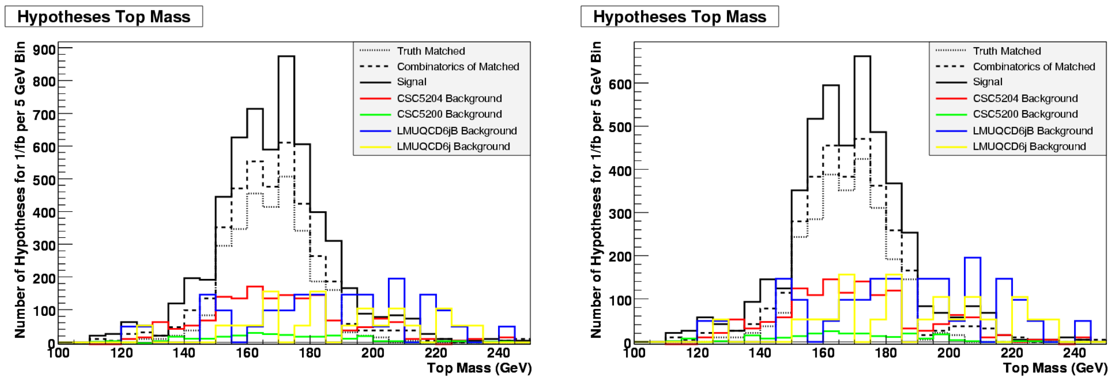

Fig. 6.4: Overlay of the various samples final mass hypotheses normalized to 1 fb^{-1}. The distributions for weight() cut of 3 and 4.7 are shown on the left and right respectively.

6.3 Top Mass Extraction

It can be seen in Fig. 6.4 that the signal and background have different shapes. As already mentioned, several of the background samples contain tops. Many of the CSC5200, CSC5204 background samples as well as the combinatorial background have one hadronic top hypothesized correctly. Of course since there is only one top it is not a Fully Hadronic $t\bar{t}$ event, even in the CSC5204 background. It is difficult to remove the good hadronic tops to see the underlying shape of the wrongly hypothesized tops. The main reason for this difficulty is that all jets are altered in the kinematic fitter in a way which correlates them together. In the case that one top was correctly assigned before the kinematic fitter it will be altered such that the last term in Eq. 5.2 is satisfied. The background was fit to the shape:

$$A\left[e^{-\frac{(x-B)^2}{2C^2}} + De^{-\frac{(x-B-E)^2}{2F^2}}\right]. \tag{6.1}$$

Table 6.3: Fixed values for Eq. (6.1).

C	D	E	F
20 GeV	0.55 GeV	42	14 GeV

This double Gaussian shape was chosen because there will be two peaks in the background. The CSC5200 and the CSC5204 backgrounds will from a peak around the top mass. The QCD Background was found to form a peak at a somewhat higher value. Since the number of QCD events is low, the statistical error is high. The combinatorial background was not included in with the other backgrounds. It is understood that that background is top mass dependent. In order to test if this shape was appropriate it was fit to the sum of all backgrounds for a number of different modification methods. These were simple Gaussian smoothing and re-binning methods available in ROOT as well as altering the bin errors. They were tried in several combinations for several values. Once the shape was understood the constant values C through F were fixed to appropriate values listed in Table 6.3. The appropriate values were found by fitting the smoothed background distribution with the initial starting points found when all the errors where set to unity. This shape was then fit to the unaltered background distribution allowing only the constants A and B to vary. It can be seen in Fig. 6.5 that these fits are limited by the statistical error.

Generation of more events is essential if a better fit to the background shape is to be made. Since no more events are available, this shape is assumed to be correct. Polynomial shapes were also explored but rejected in favour of the shape in Eq. (6.1). The polynomial shapes were very similar to the chosen shape except that there was poor behaviour at the edges.

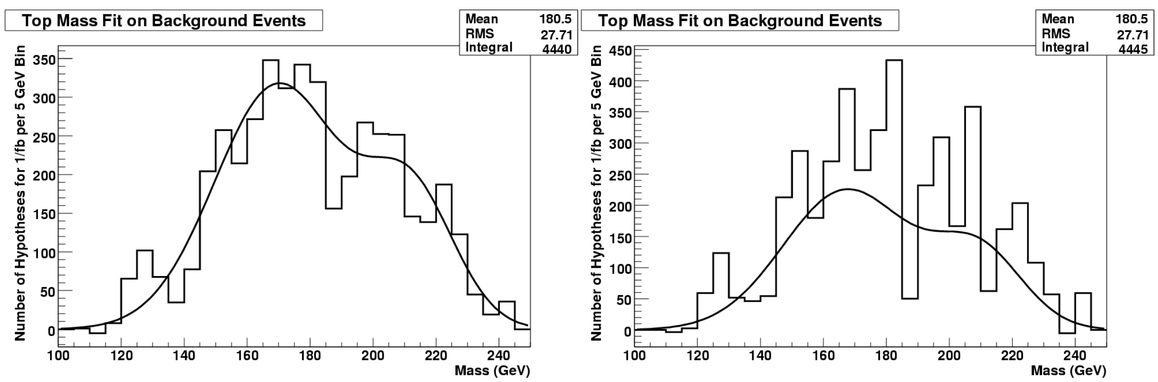

Fig. 6.5: The shape of Eq. (6.1) fit to the sum of all backgrounds for the pessimistic scenario. The left plot shows the fit where all variables were able to vary on a smoothed background. The right shows where only values A and B were allowed to vary since the others were fixed according to Table 6.3.

The Signal and Truth Matched samples can be fit to a Gaussian of the form:

$$\beta e^{-\frac{(x-\mu)^2}{2\sigma^2}}. \tag{6.2}$$

A Gaussian was chosen over a Breit-Wigner because the large error in the jets will dominate the shape. It can be seen in Fig. 6.6 that a Gaussian is an appropriate shape to fit to the mass peak.

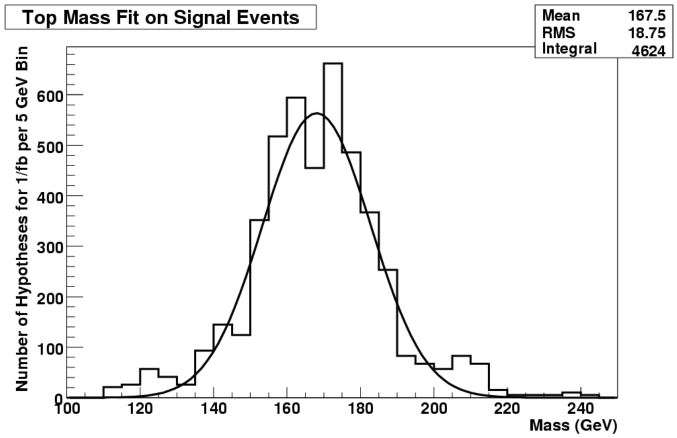

Fig. 6.6: Gaussian fit to the Signal for the pessimistic scenario.

The Truth Matched sample was also fit to a Gaussian for comparison. As was already apparent in Fig. 6.4, the combinatorial background forms small shoulders on either side of the true peak. They are now emphasized in the fit shown in Fig. 6.6 because the shoulders rise significantly above the Gaussian shape. Table 6.4 shows the values for the Gaussian fits done. All of these fits give low top mass values when compared to the generated value of 174 GeV.

Table 6.4: Fit values for the top mass peak.

Sample	μ GeV	σ GeV	β
	For weight()	**cut at 3**	
Truth Matched	167.50 ± 0.22	11.59 ± 0.16	487.24 ± 11.4
Signal	168.37 ± 0.21	15.19 ± 0.19	703.57 ± 13.1
	For weight()	**cut at 4.7**	
Truth Matched	166.63 ± 0.23	10.56 ± 0.15	435.86 ± 10.9
Signal	168.06 ± 0.23	14.72 ± 0.23	563.75 ± 12.3

In an experimental situation all events would be indistinguishable since we would not have the luxury of knowing which Monte Carlo sample they came from. Therefore to extract a mass we try to fit all samples added together to the sum of these two shapes, one for signal and one for background. It is assumed that the shape in Eq. (6.1) with the values in Table 6.3 is a good approximation to the background. The height scale (A) and position (B) are all that should be varied in the background fit. The results are give in Table 6.5.

Table 6.5: Values for the fit to the signal and the background for the shapes in Eq. (6.2) and Eq. (6.1) added.

Sample	μ GeV	σ GeV	β	A	B GeV
	For weight()	**cut at 3**			
All Samples	168.94 ± 0.33	12.00 ± 0.35	713.1 ± 19.2	415.5 ± 12.0	164.87 ± 0.47
	For weight()	**cut at 4.7**			
All Samples	169.11 ± 0.36	11.03 ± 0.32	579.9 ± 18.7	380.0 ± 9.8	164.35 ± 0.39

These top mass values of about 169 GeV are low when compared to the value of 174 GeV which it was generated with. This is mainly due to the lack of b-jet energy scale calibration. Energy calibration should be done differently for b-jets than for light jets. All the jets in this analysis were calibrated as if they were light jets. Additionally, only the light jets from the W were calibrated in the kinematic fitter. A simple function based on Monte Carlo could be made to return b-jets with a more accurate calibration. Other analyses, done on the top mass in the Semileptonic channel, find a similar value [47]. Although the measured value was low it nearly matched the value obtained when the true jets were used. This implies that if the energy scale issue is resolved then the measurement will be accurate. Fig. 6.7 shows the fit to all events by the sum of the two shapes.

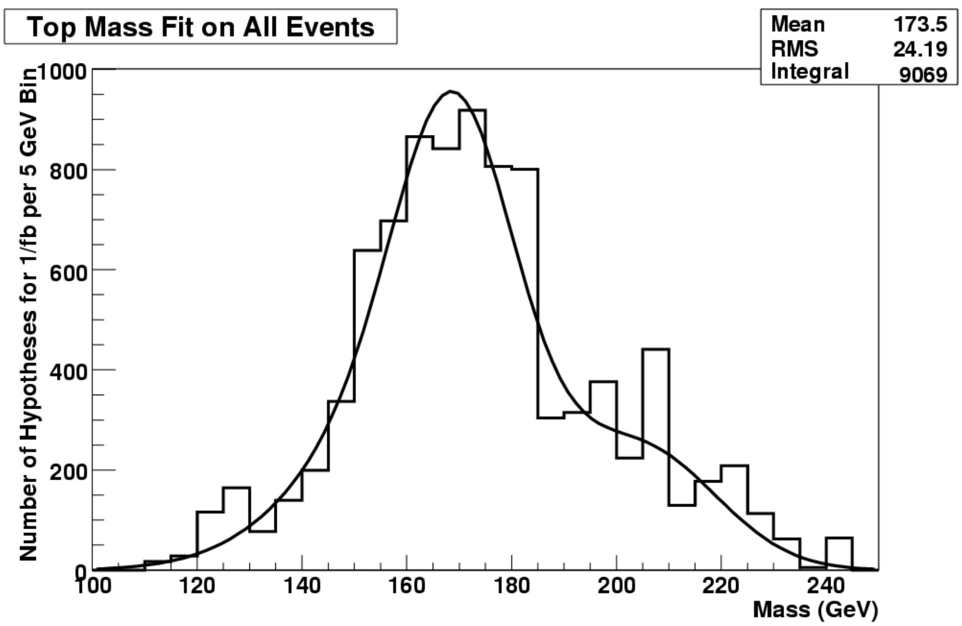

Fig. 6.7: Fit to the signal and the background for the shapes in Eq. (6.2) and Eq. (6.1) added, for the pessimistic scenario. Refer to Table 6.5 for the values for this fit.

6.4 Suggestions for Further Improvement

As with all work of this nature there are time constraints. Not all good ideas were attempted and some good ideas only became apparent when it was too late to change the analysis. Therefore, an outline of the major improvements that I believe will assist in this measurement will be given here.

In this analysis, it was required that all the 6 quarks form distinct jets; this does not need to be compulsory. An analysis could be done with many different reconstruction patterns. It could turn out that an analysis where the W's were always reconstructed as one jet is a better method. It is also possible to explore possibilities where one of the good jets was not recorded. Such a case is possible if it is out of the η range.

Splitting merged jets is also something which could be explored. This would in turn improve the matching efficiencies as less truth particles would be matched to the same jet.

All of these signal selection criteria are strongly dependent on the choice of jet finding algorithm. The choice of jet finding algorithm was predominantly made because Cone4Tower is the standard. It is likely that this is not the most efficient algorithm. Some work has been put into exploring this but without background simulated with all jet algorithms a sound statement cannot be made. The number of events passing a full analysis for Truth Matched jets and Signal are in Table 6.6. None of the analysis was changed despite the possibility of a change in optimized values of cuts for different algorithms. The purity obtained with each jet finder is approximately the same but the number of events varies. This implies that changing jet finder will not help to suppress combinatorial background but may help to suppress true background.

Table 6.6: Purity is the the percentage of correct hypotheses.

Algorithm	Cone4Tower	Cone4Topo	kT4Tower	kT4Topo	kT6Tower	kT6Topo
# Signal Hypotheses	447	460	494	500	571	579
# Truth Hypotheses	244	246	248	268	285	323
% Purtiy	54.6	53.5	50.2	53.6	49.9	55.8

It is understood that the kinematic method used could be improved. In Eq. (5.2) the mass peaks are assumed to have a Gaussian distribution. A proper Breit-Wigner form could be used, but this should only be a minimal improvement. Also, the top mass was generated as a δ function not a Breit-Wigner. We took $\Gamma_{t_o} = 0.1$ GeV to approximate the delta function. This method was written as a C^{++} class in ROOT with the minimization being done by TMinuit. There are currently other kinematic fitters being developed specifically for ATLAS analysis. The minimization is likely to be more stable than TMinuit, although when ported to Athena, the same results were obtained as in ROOT. An Athena based analysis would be preferred.

The most advanced of these other kinematic fitters is HitFit [48]. It is a kinematic fitting program which was written into Athena concurrently to the writing of this thesis. It was planned to be used originally, but it proved to be ill advised for a number of timing reasons. In further analysis, this should be used.* The algorithm was written for the Semileptonic channel but was written such that altering it to work in the Fully Hadronic channel should be possible. It is not known if it will give better results than the kinematic fitter outlined in this thesis, but there would still be several advantages, such as speed and stability.

The b-tagging weight, weight(), was not optimized to tag b-jets in this channel. The importance of each component that goes into the combined weight can be optimized for a specific sample. A specialized likelihood significance for this channel could be written to improve the efficiency. Also, the value for the weight() cut could

*It can be found at offline/PhysicsAnalysis/TopPhys/HitFit.

be optimized if fully simulated backgrounds were available.

Recent developments in basic analysis models show that much power can be gained by using decision trees instead of hard cuts. A binary decision tree shows several advantages even over a neural net [49]. Binary decision trees are not black boxes like a neural net, and as such, the error analysis is greatly simplified. A decision tree method was recently used at DO to find the single top. For more information refer to [50]. Employing this method will surely give better results.

It is believed that the general framework for this analysis is the correct scheme for top mass measurement through the Fully Hadronic channel. Changing fitting packages and jet finders may yield some more precise results but it is doubtful a complete revamp of the analysis will outperform this method. Methods on the 4-jet topology $t\bar{t} \rightarrow (bW)(bW)$ may be useful compliments to this strategy but are not expected to provide better top mass resolution.

Chapter 7

Conclusion

This thesis outlined the prospects for the measurement of the top mass through the Fully Hadronic decay of top-antitop pairs. The Fully Hadronic decay is the chain were each top decays to a W and a bottom then each W subsequently decays to a pair of quarks. This has been studied using simulated proton-proton collisions inside the ATLAS detector. The cut based analysis used a kinematic fit which constrains the jets from the W to give the W mass. Each jet assignment hypothesis was considered resulting in many possible hypotheses per event.

b-tagging is the ability to distinguish bottom flavoured jets from other jets. Methods without b-tagging were explored but did not show promise. With b-tagging a clear discrimination of signal and background was shown. Many signal events were selected for only 1 fb^{-1} implying a strong possibility for a measurement within a few fb^{-1}. An overall selection efficiency between 1.4% and 1.1% is expected for this analysis.

A top mass peak can clearly be seen for both the b-tagging values explored. A top mass of 168.94 $\pm$ 0.33(stat) GeV and 169.11 $\pm$ 0.36(stat) GeV can be extracted with the standard and pessimistic scenarios respectively. The top mass of 169 GeV is low when compared to the value of 174 GeV which it was generated with. It is likely that much of this bias is due to the lack of b-jet energy scale calibration. A more complete analysis would need to incorporate b-jet scale calibration, and a study of systematic repercussions affecting the top mass measurement.

Bibliography

[1] D.J. Griffiths. "Introduction to Elementary Particles" John Wiley & Sons, Inc., 1987.

[2] LHC Conceptual Design Report, CERN/AC/95-05, 1995.

[3] The LHC Study Group. Design study of the large hadron collider (LHC). CERN/91-03, May 1991.

[4] http://visits.web.cern.ch/visits/guides/tools/manual/english/Atlas.html

[5] Tao Han,arXiv:hep-ph/0508097v1

[6] ATLAS Collab., "ATLAS detector and Physics Performance Technical Design Report", CERN LHCC 99-14/15 (1999)

[7] U.Amaldi. Fluctuations in calorimetry measurements. "Physica Scripta, Volume 23: 409-424, 1981.

[8] C. Fabjan. "Experimental Techniques in High Energy Physics: Calorimetry in high-energy physics". Adison-Wesley, 1987.

[9] D. E. Groom et al. Review of particle physics. "The European Physical Journal", C15, 2000.

[10] R. Wigmans. On the Energy Resolution of uranium and other Hadron Calorimeters. "Nuclear Instrumentation Methods", A259: 389-429, 1987.

[11] F. Abe et al., Phys. Rev. Lett. 74, 2626 (1995)

[12] S. Abachi et al., Phys Rev. Lett. 74, 2632 (1995)

[13] The LEP Electroweak Working Group and the SLD Heavy Flavor Group, CERN-EP/99-15; D.G.Charlton, hep-ex/9912019; M.L. Swartz, hep-ex/9912026

[14] Jean-Francois Arguin PHD Thesis fermilab-thesis-2005-63

[15] M. C. Smith, S. S. Willenbrock, Phys. Rev. Lett. 79, 3825 - 3828 (1997)

[16] The 2007 PDG.

[17] N. Kidonakis R. Vogt, Phys. Rev. D 68: 114014, 2003.

[18] S. L. Glashow, J. Iliopoulos and L. Maiani, Phys. Rev. D 2, 1285 (1970).

[19] S.Eidelman et al., Phys. Lett. B 592, 1 (2004).

[20] CERN Yellow Report 2000-004, 9 may 2000, edited by G. Altarelli and M.L. Mangano, top physics chapter, page 23

[21] E. H. Simmons, hep-ph/9908511 (1999)

[22] S. P. Martin, hep-ph/9709356 (1997).

[23] B.C.Allanach et al., Eur.Phys.J. C25 (2002) 113-123; hep-ph/0202233

[24] C. T. Hill and E. H. Simmons, Phys. Rept. 381, 235 (2003)/ arXiv:hep-ph/0203079

[25] C. T. Hill Phys. Lett. B266, 419 (1991), arXiv:hep-ph/9411426 V2 2 Dec 1994.

[26] F. Abe et al., CDF Collaboration, Phys. Rev. Lett.79 (1997) 1992

[27] T. Aaltonen et al., CDF Collaboration, arXiv:0706.3790v1 [hep-ex] 26 June 2007

[28] B.Abbott et al., D0 Collaboration, Phys. Rev. D 60 (1999)012001; B.Abbott et al., D0 Collaboration, Phys. Rev.Lett. 83 (1999) 1908; hep-ex/9901023

[29] L. Simic et al., ATLAS Internal Note ATL-PHYS-2002-009

[30] Borjanovic et al., ArXiv:hep-ex/0403021 v1

[31] This is being explored thoroughly by Sander Klous of NIKHEF. No references exist at the time of this publication.

[32] L. M. Carpenter, D. E. Kaplan, E. Rhee arXiv:hep-ph/0607204v3

[33] ATLAS workbook, twiki.cern.ch/twiki/bin/view/Atlas/WorkBook

[34] T. Sjostrand, S.Mrenna, P. Skands, PHYTHIA 6.4, arXiv:hep-ph/0603175, 2006.

[35] G. Corcella, I. G. Knowels, G. Marchesini, S. Moretti, K. Odagiri, P. Richardson, M. H. Seymour, B.R. Webber, HERWIG 6.5 arXiv:hep-ph/oo11363 v3, 2002

[36] Jimmy Group, http://projects.hepforge.org/jimmy/

[37] M. L. Mangano, Fulvio Piccinini, A. D. Polosa. M. Moretti, R. Pittau, hep-ph/0206293 Version update: V2.1, December 2006

[38] S. Frixione, B. R. Webber, The MC@NLO 3.3 Event Generator, Cavendish-HEP-06/28,2006

[39] H. Baer et al, Les Houches Guidebook to Monte Carlo Generators for Hadron Collider Physics, arXiv:hep-ph/0403045 v1, 2004

[40] GEANT4 Collaboration, GEANT4: a simulation toolkit, Nuclear Instruments and Methods A, Volume 506, 2003

[41] Fyodor Tkachov Int. Journal of Mod. Phys. A, Vol 17, No 21 (2002) 2783-2884

[42] The Flavour Tagging working group. https://twiki.cern.ch/twiki/bin/view/Atlas /FlavourTagging

[43] CSC Group https://twiki.cern.ch/twiki/bin/view/Atlas/CSCEventGeneration

[44] M. Lambacher; O. Biebel; F. Fiedler, Generation of QCD multi-jet background events with ALPGEN version 2.03 and ATLFAST version 11.0.41; ATL-COM-PHYS-2007-017; Geneva : CERN, 15 Mar 2007

[45] Created by Ketevi A. Assamagan. It can be found in offline/PhysicsAnalysis /AnalysisCommon/UserAnalysis.

[46] This work has pioneered by Eric Cogneras but has not been documented at the time of this thesis.

[47] For example see AkiraShibata's talk at http://indico.cern.ch/conferenceDisplay.py ?confId=15661

[48] The method and algorithm was developed by Scott Snyder in his PhD thesis. This was then ported to Athena by Christian Schmitt as HitFit.

[49] D. Bowser-Chao and D.L. Dzialo, Phys. Rev. D 47, 1900 (1993).

[50] L. Breiman et al., Classification and Regression Trees (Wadsworth, Stamford, 1984)

Chapter 8

Appendix A

Several samples that could still be a background were not used in the final analysis due to a lack of statistics. Some more are now given in Table 8.1. The QCD multi-jet background has an increasingly high cross section as the number of jets decrease. Although fewer events will have enough jets to pass the analysis, the larger cross sections make it possible for them to be important backgrounds.

Table 8.1: The cut flow for this analysis of the unused samples.

Sample	QCD4j Bkgrnd	QCD4jB Bkgrnd	QCD3j Bkgrnd
Cross Section (pb)	480000	69000	4766000
# of Events	210000	38000	162878
After Event 1	20	2	0
After Event 2	20	2	0
After Event 3	20	2	0
After Event 4	20	2	0
After Event 5	20	2	0
Event Efficiency (%)	0.0095	0.0053	-
# of Hypotheses	1800	180	0
After Hypothesis 1	1056	78	0
After Hypothesis 2	804	60	0
After Hypothesis 3	130	6	0
After Hypothesis 4	24	0	0
After Hypothesis 5	21	0	0
After Hypothesis 6	9	0	0
After Hypothesis 7	6	0	0
After Hypothesis 8	6	0	0
After Hypothesis 9	6	0	0
After Hypothesis 10	1	0	0
After Hypothesis 11	0	0	0
After Hypothesis 12	0	0	0
Hypothesis Efficiency	-	-	-